Table 1
Distribution of PIM-1, PAX-5, RhoH/TTF, c-MYC and BCL-6 mutations in thyroid lymphomas and chronic lymphocytic thyroiditis.

Histology	Mutated/tested (%)					
	c-MYC exon 1 and 2	RohH/TTF	PIM-1	PAX-5	Any	BCL-6
CLTH	1/14 (7.1%)	1/14 (7.1%)	0/14	0/14	2/14 (14.3%)	2/14 (14.3%)
Lymphoma (all)	11/33 (33.3%)	7/33 (21.2%)	7/33 (21.2%)	2/33 (6.1%)	16/33 (48.5%)a	22/33 (66.7%)a
FL	7/11 (63.6%)a,b	7/11 (63.6%)a,b,c	5/11 (45.5%)a,b	1/11 (9.1%)	11/11 (100%)a,b,c	8/11 (72.7%)a
MZBCL	1/10 (10.0%)	0/10	0/10	0/10	1/10 (10.0%)	5/10 (50.0%)
DLBCL	3/12 (25.0%)	0/12	2/12 (16.7%)	1/12 (8.3%)	4/12 (33.3%)	9/12 (75.0%)a

CLTH, chronic lymphocytic thyroiditis; FL, follicular lymphoma; DLBCL, diffuse large B-cell lymphoma; MZBCL, merginal zone B-cell lymphoma.
a, vs chronic lymphocytic thyroiditis; b, vs MZBCL; c, vs DLBCL; statistically significant by Chi-square test.

Table 2
Mutational analysis of c-MYC, RhoH/TTF, PAX-5, and PIM-1 in thyroid lymphomas and chronic lymphocytic thyroiditis.

Patients	Age (y)/sex	Histology	c-MYC exon 1 and 2	RohH/TTF	PIM-1	PAX-5
Malignant lymphoma						
F1	73F	FL	T2501A, C2510T, G2529A, G2588A, G2611C, G2615T A2684G, A2695C, A2742G, G2777T, A2825C, T2853G G2866C, C2887T, T2913C, C2934A, T2976C, C2984G C2991G, C2993T, T2999C, C3065G, G3073A, G3089A C3158A, C3186G, T3191C, C3267G, C3331T, (C4807G)	G368T	G2497GA	–
F2	48F	FL	–	C448T	–	–
F3	54F	FL	A3045G	–	–	–
F4	59F	FL	G3035T	A460G	–	–
F5	60F	FL	(G5213A)	–	A2634T	–
F6	71F	FL	(T5236C)	–	G2050A	–
F7	50F	FL	G3035T	A1021T, del 701–1004	–	–
F8	66F	FL	(T4465C)	–	G2715A	–
F9	69F	FL	–	C838T	–	G812T
F11	67F	FL	–	G351C, A642C	–	–
F12	79M	FL	–	G698C, T710C	del2425–27	–
M1	76F	MZBCL	–	–	–	–
M2	65M	MZBCL	–	–	–	–
M3	73F	MZBCL	–	–	–	–
M4	67M	MZBCL	–	–	–	–
M5	70F	MZBCL	–	–	–	–
M6	73M	MZBCL	(G5213A)	–	–	–
M7	72F	MZBCL	–	–	–	–
M8	56F	MZBCL	–	–	–	–
M9	85F	MZBCL	–	–	–	–
M10	66M	MZBCL	–	–	–	–
D1	45F	DLBCL	G3035T	–	–	–
D2	61F	DLBCL	–	–	–	–
D3	67M	DLBCL*	–	–	–	–
D4	89F	DLBCL	C2879T, 3439del 8 bp	–	–	C1000T
D5	80F	DLBCL	–	–	–	–
D6	27F	DLBCL	–	–	–	–
D7	71F	DLBCL	–	–	–	–
D8	68F	DLBCL	–	–	–	–
D11	60F	DLBCL*	(C4498G)	–	C2757A	–
D12	60F	DLBCL	–	–	–	–
D13	81M	DLBCL*	–		–	–
D14	74F	DLBCL	–	–	A2634G	–
Chronic lymphocytic thyroiditis						
H1	50F		–	T420C	–	–
H2	57F		–	–	–	–
H3	55F		–	–	–	–
H4	67F		–	–	–	–
H5	66F		–	–	–	–
H6	61F		–	–	–	–
H7	68F		(T5338C)	–	–	–
H8	70F		–	–	–	–
H9	75F		–	–	–	–
H11	66F		–	–	–	–
H12	52F		–	–	–	–
H13	66M		–	–	–	–
H14	45F		–	–	–	–
H15	75F		–	–	–	–

FL, follicular lymphoma; DLBCL, diffuse large B-cell lymphoma; MZBCL, marginal zone B-cell lymphoma; *, germinal center B-cell-like phenotype.
Numbered according to GenBank accession numbers X00364 (c-MYC), AF386789 (RhoH/TTF), AF386792 (PIM-1), and AF386791 (PAX-5).
del, deletion; mutation located in exon 2 of c-MYC was shown in parenthesis.

Table 3
Summary of PIM-1, PAX-5, RhoH/TTF, c-MYC and BCL-6 mutations in thyroid lymphomas and chronic lymphocytic thyroiditis.

Gene	Mutation frequency/1000 bp		Insertion/deletion		Single bp substitution		Transitions/Transversions		G+C/A+T		RGYW	
	CLTH	TL	CLTH	TL	CLTH	TL	CLTH	TL	CLTH	TL	CLTH	TL
c-MYC												
exon1	0	4.35 (0.77–22.27)	0/0	0/1	0	34	0/0	16/18	0/0	23/11	0	14 (*p=0.023)
exon2	0.86	0.86	0/0	0/0	1	6	1/0	4/2	0/1	4/2	0	1
RHOH/TTF	1.13	1.46 (1.13–2.26)	0/0	0/1	1	9	1/0	4/5	0/1	5/4	0	0
PIM-1	0	0.98	0/0	0/1	0	7	0/0	4/2	0/0	4/2	0	3
PAX-5	0	1.1	0/0	0/0	0	2	0/0	1/1	0/0	2/0	0	2
All genes	NA	NA	0/0	0/3	2	58	2/0	29/28	0/2	38/19	0	20
BCL-6	2.71 (1.35–4.06)	8.38 (1.35–20.30)	0/0	0/6	4	130	4/0	59/81	0/4	63/67	1	32 (*p=0.033)

CLTH, chronic lymphocytic thyroiditis; TL, thyroid lymphoma.
* Significant by Chi-square test.

of 10 in MZBCL (50.0%) (Tables 1 and 4). Frequency of mutations was not significantly different between GC (2 of 3 (66.7%)) and non-GC (7 of 9 (77.8%)) subtypes in DLBCL. Mutation frequency for ASHM in *PAX-5* (1.1/1000 bp), *c-MYC exon 1* (1.1/1000 bp), *c-MYC exon 2* (0.86/1000 bp), *PIM-1* (0.98/1000 bp), and *RhoH/TTF* (0.98/1000 bp) was generally lower than that for SHM in BCL-6 sequences (8.38/1000 bp) in TL. Of the 130 single base-pair substitutions identified in the 33 specimens, 59 were transitions and 81 transversions, with a transition-to-transversion ratio of 0.73 (expected 0.5, $p = 0.13$, Chi-square test; Table 3). Mutations predominantly involved the RGYW/WRCY motifs ($p = 0.03$) (Table 3).

3.4. Clonality analysis of PIM-1, PAX-5, RhoH/TTF, and c-MYC

To investigate whether ASHM in TL is ongoing, clonality analysis for estimation of intraclonal heterogeneity was performed in 10 TL, consisting of 7 FL (F1, F5, F7, F8, F9, F11, F12) and 3 DLBCL (D4, D11, D14) with mutations in PIM-1, PAX-5, or RhoH/TTF by direct sequencing. In all tumors analyzed, 1 or 2 predominant alleles recapitulated the mutations observed by direct sequencing of the PCR product, confirming their presence in the tumor (not shown). A intraclonal variants were found in 3 of 7 FL and 1 of 3 DLBCL.

For comparison, clonality analysis of *BCL-6* gene was performed in 9 TL including of 3 FL (F1, F8, F9), 3 MZBCL (M3, M5, M8) and 3 DLBCL (D1, D2, D11). Intraclonal variants were found in 2 of 3 FL, 2 of 3 MZBCL and 3 of 3 DLBCL, respectively. A large number of intraclonal variants were found in 5 of these cases (F1, F9, D2, D9, M3). These data indicate that ASHM activity may be ongoing in a fraction of FL and DLBCL.

3.5. AID and POL-eta expression

AID and *POL-eta* are cellular gene products playing central roles in the DNA-modifying processes during immunoglobulin gene class switch recombination and SHM [8,9]. Expression level of AID was significantly higher in TL than in CLTH (Fig. 1), but was various among cases with TL. Expression level of AID was highest in DLBCL, followed by MZBCL and FL in order. Expression level of AID in ASHM negative cases was higher than that in ASHM positive cases, but statistically not significant ($p = 0.092$). Expression level of POL-eta was almost similar between TL and in CLTH, ASHM negative and positive cases, and among each histological type (data not shown).

4. Discussion

Occurrence of ASHM is initially regarded as a characteristic feature for nodal DLBCL based on the observation in systemic B-cell lymphomas [3]. Subsequent study demonstrated that ASHM also occurred in extra-nodal DLBCL of specific category such as AIDS-related [4], central nerves system [5], and mediastinal diseases [6,7]. ASHM was also found in FL [9,11]. ASHM occurred in both MZBCL and extranodal DLBCL, and suggested a role of ASHM for transformation from MZBCL to DLBCL [10]. Taken together, ASHM is supposed to contribute to lymphomagenesis in GC B-cell origin through induction of genome wide genetic instability covering multiple loci even outside the Ig genes, including c-MYC, *RhoH/TTF*, *PAX-5* and *PIM-1* proto-oncogenes. In addition, ASHM may induce occurrence of chromosomal translocations because the process of SHM is intrinsically associated with DNA double-strand breaks [3].

This study on TL revealed another aspects of ASHM as summarized below. (1) Involvement of ASHM with *PIM-1*, *RhoH/TTF*, and *c-MYC* was not so frequent in DLBCL of TL (4 (33.3%) of 12 cases), as reported previously for DLBCL in the different settings, i.e., nine (90%) of ten primary central nervous system lymphomas [5], 17 (100%) of 17 with extranodal DLBCLs [10], 10 (55.6%) of 18 AIDS-DLBCLs [4], and 14 (73.7%) of 19 primary mediastinal DLBCL [6,7]. (2) Involvement of ASHM with *PIM-1*, *RhoH/TTF*, and *c-MYC* was not common in MZBCL. Frequency of ASHM in MZBCL was not significantly different from that in DLBCL, which contrasts to the findings reported in the previous study by Deutsch et al. [10], i.e., ASHM was

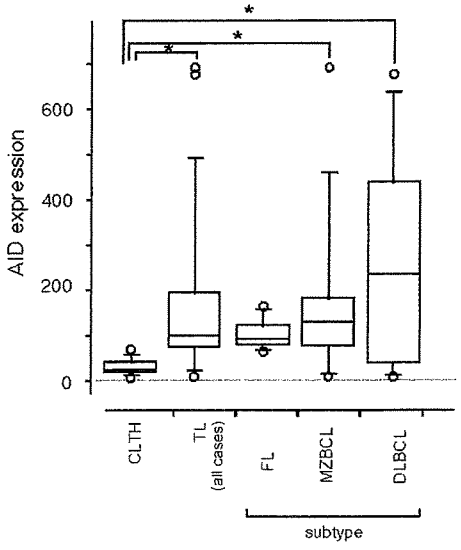

Fig. 1. *AID* expression in CLTH and ML. *AID* was expressed at significantly higher level in TL than in CLTH. Expression level of AID mRNA was highest in DLBCL, followed by MZBCL and FL.

Table 4
Mutational analysis of BCL-6 in thyroid lymohoma and chronic lymphocytic thiloiditis.

Patients	Age (y)/sex	Histology	BCL-6								
			Ins/del	Single bp substitution							
Thyroid lymphoma											
F1	73F	FL	–	G84C	T107G	C145G	T163G	G222C	T266A	C435T	C549T
				T557C	C566A	T569C	G647A	C656T			
F2	48F	FL	–	G66A	A80C	A99G	G132A	T181G	A191T	T194C	G322T
				G402C	C421A	T439C	T501G	G518A	C697T	T747A	
F3	54F	FL	–	–							
F4	59F	FL	–	G434A	G443A						
F5	60F	FL	–	–							
F6	71F	FL	–	T143C	G184C	G416T					
F7	50F	FL	–	–							
F8	66F	FL	del 132–478	C88G	A112G	T581G	T592C	G719C			
F9	69F	FL	–	G122C	G177C	A181G	G193A	T194C	G234A	C459G	T478A
F11	67F	FL	del 186–207	–							
F12	79M	FL	–	T247C	G347C						
M1	76F	MZBCL	–	–							
M2	65M	MZBCL	–	–							
M3	73F	MZBCL	–	G122C	C158T	T197G	C486G				
M4	67M	MZBCL	–	–							
M5	70F	MZBCL	del 173–418	T76C	C123T	C435T	G441C	C452G	T480G	C561T	A716G
M6	73M	MZBCL	–	A174G	T456A	C543A					
M7	72F	MZBCL	–	–							
M8	56F	MZBCL	del 90–454	T481A	T496C	C510T	G597A	T632A	T758C		
M9	85F	MZBCL	–	–							
M10	66M	MZBCL	del 429–534	A86T	G122A	G184A	A191C	A205T	T207C	C228G	A600G
				T645C	T687C	T745A					
D1	45F	DLBCL	del 97–479	T570G	T572A	G691T	A716G	A749T			
D2	61F	DLBCL	–	T89C	A99C	T107C	C123G	A191C	G369C	T517G	C544A
				T595C	T599A						
D3	67M	DLBCL*	–	C88T	T131A	G288C	A311T	T546C	T729C		
D4	89F	DLBCL	–	G294A	A344G	A506G					
D5	80F	DLBCL	–	G431A							
D6	27F	DLBCL	–	A72C	A90T	G184C	A205G	G211C	G229A	C490G	C519A
				C591G	C631A						
D7	71F	DLBCL	–	–							
D8	68F	DLBCL	–	T105A	C123G	A727G	G735C				
D11	60F	DLBCL*	–	T194C	C421A	T439C	T501G	G518A	C698T	T747A	
D12	60F	DLBCL	–	–							
D13	81M	DLBCL*	–	–							
D14	74F	DLBCL	–	T105A	G122C	T204G					
Chronic lymphocytic thiloiditis											
H1	50F		–	–							
H2	57F										
H3	55F		–	–							
H4	67F		–	–							
H5	66F		–	–							
H6	61F		–	–							
H7	68F		–	–							
H8	70F		–	T541C							
H9	75F		–	T600C	A645G	A710G					
H11	66F		–	–							
H12	52F		–	–							
H13	66M		–	–							
H14	45F		–	–							
H15	75F		–	–							

FL, follicular lymphoma; DLBCL, diffuse large B-cell lymphoma; MZBCL, marginal zone B-cell lymphoma; *, germinal center B-cell-like phenotype; del, deletion. Numbered according to GenBank accession numbers AF191831 (BCL-6).

common in MZBCL (13 (76.5%) of 17 cases) but was much higher in DLBCL. They include lymphoma of various origins, such as stomach, orbita parotid gland, soft tissue and several thyroids. In our study, samples were derived from only thyroid using snap-frozen tissue. Libra et al. [8] reported that ASHM may not contribute significantly to both HCV-associated DLBCL and MZBCL. It is possible that the contribution of ASHM to lymphomagenesis in DLBCL and MZBCL may differ among the sites and the underlying disease derived from. (3) Involvement of ASHM with *PIM-1*, *RhoH/TTF*, and c-*MYC* was common in FL of TL (all of 11 cases), which was significantly higher than that in other kinds of TL ($p < 0.05$). Furthermore, the mutations found in c-MYC and PIM-1 in 2 cases of FL supposed to cause amino acid change. Whereas, involvement of ASHM with nodal FL was rare in the original report by Pasqualucci et al. [3], and it was found in 10 (53%) of 19 primary cutaneous FL [9] and 75–77% of FL [11]. (4) FL of thyroid was also unique in its lower level of AID expression compare to DLBCL and MZBCL. Expression level of AID gene was not correlated with the frequency of ASHM in the present series which is in consistent with the previous report [27].

ASHM has so far never been described in non-lymphoma tissues. It is somewhat unexpected that ASHM was found in a fraction of CLTH. We have confirmed the reactive and non-neoplastic nature of CLTH lesions by clonality assays [24,26]. There are at least three possible explanations for this discrepancy. The first is that ASHM

may really occur in CLTH. The second is that the nucleotide change may result from polymorphysm but not ASHM. The other possibility is that the lesions are mixture of CLTH and lymphoma that has just arisen from the CLTH. Further analysis may be necessary for discriminating these possibilities.

TL is one of well-known type of lymphomas developing in mucosa-associated lymphoid tissue, but information for molecular genetic features of TL was quite limited until present. Present data provide an insight about the oncogenesis of TL, i.e., ASHM may play a role in the development of FL, while not so much in MZBCL. DLBCL consists of ASHM negative and positive cases, indicating the heterogeneous character of this lymphoma. ASHM negative DLBCL cases may be derived from a MZBCL/DLBCL axis or de novo and not from the transformed FL. As for ASHM positive DLBCL, three possibilities must be taken into account: the first is transformation of FL to DLBCL, the second is increase of ASHM during transformation of MZBCL to DLBCL, and the third is DLBCL arising de novo.

Conflict of interest

None.

Acknowledgement

Supported by grants from the Ministry of Education, Science, Culture, and Sports, Japan (14031213, 14770073, 15026209, 15406013, 15590340, 16390105, 18014015).

References

[1] Kuppers R, Klein U, Hansmann ML, Rajewsky K. Cellular origin of human B-cell lymphomas. N Engl J Med 1999;341:1520–9.
[2] Shen HM, Peters A, Baron B, Zhu X, Storb U. Mutation of BCL-6 gene in normal B cells by the process of somatic hypermutation of Ig genes. Science 1998;280:1750–2.
[3] Pasqualucci L, Neumeister P, Goossens T, Nanjangud G, Chaganti RS, Kuppers R, et al. Hypermutation of multiple proto-oncogenes in B-cell diffuse large-cell lymphomas. Nature 2001;412:341–6.
[4] Gaidano G, Pasqualucci L, Capello D, Berra E, Deambrogi C, Rossi D, et al. Aberrant somatic hypermutation in multiple subtypes of AIDS-associated non-Hodgkin lymphoma. Blood 2003;102:1833–41.
[5] Montesinos-Rongen M, Van Roost D, Schaller C, Wiestler OD, Deckert M. Primary diffuse large B-cell lymphomas of the central nervous system are targeted by aberrant somatic hypermutation. Blood 2004;103:1869–75.
[6] Bödör C, Bognár A, Reiniger L, Szepesi A, Tóth E, Kopper L, et al. Aberrant somatic hypermutation and expression of activation-induced cytidine deaminase mRNA in mediastinal large B-cell lymphoma. Br J Hematol 2005;129:373–6.
[7] Rossi D, Cerri M, Capello D, Deambrogi C, Berra E, Franceschetti S, et al. Aberrant somatic hypermutation in primary mediastinal large B-cell lymphoma. Leukemia 2005;19:2363–6.
[8] Libra M, Capello D, Gloghini A, Laura P, Berra E, Cerri M, et al. Analysis of aberrant somatic hypermutation (SHM) in non-Hodgkin's lymphomas of patients with chronic HCV infection. J Pathol 2005;206:87–91.
[9] Dijkman R, Tensen CP, Buettner M, Niedobitek G, Willemze R, Vermeer MH. Primary cutaneous follicle center lymphoma and primary cutaneous large B-cell lymphoma, leg type, are both targeted by aberrant somatic hypermutation but demonstrate differential expression of AID. Blood 2006;107:4926–9.
[10] Deutsch AJ, Aigelsreiter A, Staber PB, Beham A, Linkesch W, Guelly C, et al. MALT lymphoma and extranodal diffuse large B-cell lymphoma are targeted by aberrant somatic hypermutation. Blood 2007;109:3500–4.
[11] Halldórsdóttir AM, Frühwirth M, Deutsch A, Aigelsreiter A, Beham-Schmid C, Agnarsson BA, et al. Quantifying the role of aberrant somatic hypermutation in transformation of follicular lymphoma. Leuk Res 2008;32:1015–21.
[12] Freeman C, Berg JW, Cutler SJ. Occurrence and prognosis of extranodal lymphomas. Cancer 1972;29:252–60.
[13] Aozasa K, Tsujimoto M, Sakurai M, Honda M, Yamashita K, Hanada M, et al. Non-Hodgkin's lymphomas in Osaka. Japan Eur J Cancer Clin Oncol 1985;21:487–92.
[14] Volpe R. Thyroiditis: current views of pathogenesis. Med Clin North Am 1975;59:1163–75.
[15] Kato I, Tajima K, Suchi T, Aozasa K, Matsuzuka F, Kuma K, et al. Chronic thyroiditis as a risk factor of B-cell lymphoma in the thyroid gland. Jpn J Cancer Res (Gann) 1985;76:1085–90.
[16] Jaffe ES, Harris NL, Stein H, Vardiman JW. World Health Organization classification of tumours pathology and genetics of tumours of haematopoietic and lymphoid tissues. Lyon: IARC Press; 2001.
[17] Miwa H, Takakuwa T, Nakatsuka S, Tomita Y, Matsuzuka F, Aozasa K. DNA sequence of immunoglobulin heavy chain variable region gene in thyroid lymphoma. Jpn J Cancer Res 2001;92:1041–7.
[18] Sato Y, Nakamura N, Nakamura S, Sakugawa S, Ichimura K, Tanaka T, et al. Deviated VH4 immunoglobulin gene usage is found among thyroid mucosa-associated lymphoid tissue lymphomas, similar to the usage at other sites, but is not found in thyroid diffuse large B-cell lymphomas. Mod Pathol 2006;19:1578–84.
[19] Goodman MF. Error-prone repair DNA polymerases in prokaryotes and eukaryotes. Annu Rev Biochem 2002;71:17–50.
[20] Muramatsu M, Kinoshita K, Fagarasan S, Yamada S, Shinkai Y, Honjo T. Class switch recombination and hypermutation require activation-induced cytidine deaminase (AID), a potential RNA editing enzyme. Cell 2000;102:553–63.
[21] Petersen-Mahrt SK, Harris RS, Neuberger MS. AID mutates *E. coli* suggesting a DNA deamination mechanism for antibody diversification. Nature 2002;418:99–103.
[22] Zeng X, Winter DB, Kasmer C, Kraemer KH, Lehmann AR, Gearhart PJ. DNA polymerase eta is an A-T mutator in somatic hypermutation of immunoglobulin variable genes. Nat Immunol 2001;2:537–41.
[23] Hans CP, Weisenburger DD, Greiner TC, Gascoyne RD, Delabie J, Ott G, et al. Confirmation of the molecular classification of diffuse large B-cell lymphoma by immunohistochemistry using a tissue microarray. Blood 2004;103:275–82.
[24] van Dongen JJ, Langerak AW, Bruggemann M, Evans PA, Hummel M, Lavender FL, et al. Design and standardization of PCR primers and protocols for detection of clonal immunoglobulin and T-cell receptor gene recombinations in suspect lymphoproliferations: report of the BIOMED-2 Concerted Action BMH4-CT98-3936. Leukemia 2003;17:2257–317.
[25] D'Haese JG, Tsukasaki K, Cremer FW, Fischer C, Bartram CR, Jauch A. Chromosomal aberrations in follicular non-Hodgkin lymphomas of Japanese patients, detected with comparative genomic hybridization and polymerase chain reaction analysis. Cancer Genet Cytogenet 2005;162:107–14.
[26] Yamauchi A, Tomita Y, Takakuwa T, Hoshida Y, Nakatsuka S, Sakamoto H, et al. Polymerase chain reaction-based clonality analysis in thyroid lymphoma. Int J Mol Med 2002;10:113–7.
[27] Pasqualucci L, Guglielmino R, Houldsworth J, Mohr J, Aoufouchi S, Polakiewicz R, et al. Expression of the AID protein in normal and neoplastic B cells. Blood 2004;104:3318–25.

Int. J. Cancer: **125**, 381–387 (2009)

WT1 IgG antibody for early detection of nonsmall cell lung cancer and as its prognostic factor

Yusuke Oji[1], Yayoi Kitamura[1], Eriko Kamino[2], Aiko Kitano[1], Noriyoshi Sawabata[3], Masayoshi Inoue[4], Masahide Mori[5], Shin-ichi Nakatsuka[6], Nao Sakaguchi[2], Kaori Miyazaki[2], Michiyo Nakamura[2], Ikuyo Fukuda[2], Junya Nakamura[2], Naoya Tatsumi[2], Tetsuya Takakuwa[7], Sumiyuki Nishida[8], Toshiaki Shirakata[1], Naoki Hosen[9], Akihiro Tsuboi[8], Riichiro Nezu[10], Hajime Maeda[11], Yoshihiro Oka[12], Ichiro Kawase[12], Katsuyuki Aozasa[7], Meinoshin Okumura[4], Shinichiro Miyoshi[3] and Haruo Sugiyama[2]*

[1]*Department of Biomedical Informatics, Osaka University Graduate School of Medicine, Suita, Osaka, Japan*
[2]*Department of Functional Diagnostic Science, Osaka University Graduate School of Medicine, Suita, Osaka, Japan*
[3]*Department of Cardiothoracic Surgery, Dokkyo Medical University, Tsuga-gun, Tochigi, Japan*
[4]*Department of Thoracic Surgery, Osaka University Graduate School of Medicine Suita, Osaka, Japan*
[5]*Department of Respiratory Medicine, Toneyama National Hospital, Toyonaka, Osaka, Japan*
[6]*Department of Pathology, Sumitomo Hospital, Osaka, Osaka, Japan*
[7]*Department of Pathology, Osaka University Graduate School of Medicine, Suita, Osaka, Japan*
[8]*Department of Cancer Immunotherapy, Osaka University Graduate School of Medicine, Suita, Osaka, Japan*
[9]*Department of Cancer Stem Cell Biology, Osaka University Graduate School of Medicine, Suita, Osaka, Japan*
[10]*Department of Surgery, Osaka Rosai Hospital, Sakai, Osaka, Japan*
[11]*Department of Thoracic Surgery, Toneyama National Hospital, Toyonaka, Osaka, Japan*
[12]*Department of Respiratory Medicine and Allergy, Rheumatic Disease, Osaka University Graduate School of Medicine, Suita, Osaka, Japan*

There are urgent needs to develop methods for early detection of nonsmall cell lung cancer (NSCLC) because of its increasing incidence and poor prognosis. Here, we analyzed the production of IgG antibody (WT1 Ab) against WT1 (Wilms' tumor gene) protein that was overexpressed in the majority of NSCLC. Enzyme-linked immuno-sorbent assay showed that WT1 Ab was produced in all of 91 NSCLC patients and 70 healthy individuals and that WT1 Ab titers were significantly higher in NSCLC patients compared with healthy individuals. When the cut-off level of WT1 Ab titers were fixed at mean + 3SD of those in healthy individuals, 26.4% of NSCLC patients had WT1 Ab titers over the cut-off level, and positive rates of WT1 Ab at each clinical stage were 25.0, 30.8 and 38.4% in stage I, II and III NSCLC, respectively. When WT1 Ab was combined with CEA or CYFRA for detection of NSCLC, positive detection rates increased from 25.0 to 34.1 and 31.8%, respectively, in stage I and from 38.4 to 69.2 and 46.1%, respectively, in stage III, but not changed in stage II. Western blot analysis showed that dominant subclass of WT1 Ab was Th1-type IgG2. Interestingly, elevation of WT1 Ab titers was significantly associated with longer disease-free survival in patients with stages I–III NSCLC. These results showed that WT1 Ab could be a useful marker for early detection of NSCLC and its prognostic prediction. These results also suggested that WT1-specific immune responses played an important role in anti-cancer immunity in NSCLC.

Key words: lung cancer; WT1; humoral immune response; tumor marker; prognostic marker

Lung cancer is the leading cause of cancer death in the world and nonsmall cell lung cancer (NSCLC) represents nearly 80% of the disease.[1] Because 75% of lung cancer patients are diagnosed at stages of metastatic spread when therapies are rarely curative,[2] early detection of localized lung cancer is the key to improve its clinical outcome.

Although chest X-ray is routinely used as a screening tool, its limitation to detect localized lung cancer has been evident because of its insufficient sensitivity.[2] Recently, low-dose spiral computed tomography (CT) has been proposed as an early detection screening tool. However, despite its high sensitivity, specificity of CT in lung cancer detection is poor.[3] Therefore, serum biomarkers with high sensitivity and specificity for diagnosis of lung cancer are needed. However, current serum biomarkers for NSCLC such as carcino embryonic antigens (CEA) and squamous cell carcinoma antigen do not have sufficient sensitivity and specificity required for early detection of NSCLC.[4,5]

It is now clear that malignant transformation occurs by changes in cellular gene expression with subsequent clonal proliferation. Altered gene expression in malignant cells may lead to the expression of aberrantly expressed proteins recognized by host immune system. If autoantibodies against these antigens are produced at early stage of NSCLC when quantity of the tumor antigens in the circulation is very small, these antibodies should be useful markers for early detection of NSCLC. Moreover, because production of IgG antibodies needs helper T-cell functions and helper T cells play an important role in cellular immune responses, IgG antibodies against tumor antigens may be more useful markers for predicting prognosis in NSCLC patients compared with IgM antibodies.

The *WT1* gene was originally isolated as a tumor suppressor gene responsible for a kidney neoplasm of the childhood, Wilms' tumor.[6] However, we have demonstrated that the wild-type *WT1* gene is overexpressed in leukemia[7] and various types of solid cancers including lung,[8,9] gastric,[10] esophageal,[11] colorectal[12] and pancreatic cancers.[13] We proposed that the wild-type *WT1* gene played oncogenic roles rather than tumor-suppressor functions in tumorigenesis of various types of cancers.[14–16] We had previously demonstrated that IgG and IgM Ab against WT1 were produced at higher levels in patients with AML and MDS compared with normal individuals[17] and that Th1 type subclasses of WT1 IgG Ab, IgG1, 2, and 3 were dominantly produced in the patients.[18] On the other hand, production of WT1 Ab in patients with solid tumors remained undetermined.

In the present study, we demonstrate that high titers of Th1 type WT1 IgG antibody are detected in 26.4% of NSCLC patients and positive detection rate of WT1 Ab was higher than that of CEA or CYFRA in stages I and II NSCLC. Moreover, we describe that

Grant sponsor: Ministry of Education, Science, Sports, Culture and Technology and the Ministry of Health, Labour, and Welfare, Japan.
***Correspondence to:** Department of Functional Diagnostic Science, Osaka University Graduate School of Medicine, 1-7 Yamada-Oka, Suita, Osaka, Japan. Fax: +81-6-6879-2597.
E-mail: sugiyama@sahs.med.osaka-u.ac.jp
Received 25 December 2008; Accepted after revision 3 February 2009
DOI 10.1002/ijc.24367
Published online 18 February 2009 in Wiley InterScience (www.interscience.wiley.com).

TABLE I - CHARACTERISTICS OF THE PATIENTS WITH NSCLC

	Stage				Age (median)	Sex (M:F)	Total
	I	II	III	Unknown			
Adenocarcinoma	27	5	9	13	42–83 (70)	32:22	54
Squamous Cell Carcinoma	13	6	1	9	48–85 (68)	23:6	29
Large Cell Carcinoma	4	0	0	0	63–81 (72)	4:0	4
Pleomorphic Carcinoma	1	0	1	0	60–82	2:0	2
Adeno-squamous Cell Carcinoma	0	1	1	0	74–75	1:1	2

high titers of WT1 IgG Ab are associated with longer disease-free survival (DFS) in stages I–III NSCLC.

Material and methods

Serum samples

Serum samples were obtained from 91 patients with nonsmall cell lung cancer (54 adenocarcinoma, 29 squamous cell carcinoma, 4 large cell carcinoma, 2 pleomorphic carcinoma, 2 adeno-squamous cell carcinoma) before operation and from 70 healthy individuals under written informed consent at Dokkyo Medical University Hospital, Toneyama National Hospital, Osaka Rosai Hospital and Osaka University Hospital. Characteristics of the patients are shown in Table I. The samples were stocked at −80°C until use.

Tissue samples

Tissue samples were obtained from 41 patients (40 adenocarcinoma and 1 squamous cell carcinoma) with stage I NSCLC at Osaka University Hospital under informed consent.

Construction of vectors for recombinant WT1 protein

To obtain recombinant full length WT1 protein and one each of three WT1 fragment proteins [WT-Fr1 (1–182aa), WT-Fr2 (180–324aa) and WT-Fr3 (318–449 aa)], corresponding region of the *WT1* gene was amplified by PCR using Pfx polymerase (Invitrogen, Carlsbad, CA) and inserted into the pGEX-5X-3 vector (GE Healthcare Biosciences, Piscataway, NJ) that allowed the expression of the recombinant protein with an N-terminal GST tag. GST tagged, full length WT1 protein was purified by size fractionation using NA-1800 apparatus (Nippon Eido, Tokyo, Japan) according to the manufacturer's instructions. WT1 fragment proteins and GST protein were purified using Glutathione Sepharose 4 Fast Flow beads (GE Healthcare Biosciences) according to the manufacturer's instructions.

Enzyme-linked immunosorbent assay

Enzyme-linked immunosorbent assay (ELISA) was established to measure the titers of WT1 IgG Ab present in serum from patients and healthy individuals. ELISA 96 well plates (Multi Well Plate H Type Plate MS-8896F, Sumitomo Bakelite, Japan) were coated with 100 μl of recombinant GST tagged, full length WT1 protein (20 μg/ml) in immobilization Buffer (10 mM $NaCO_3$, 30 mM $NaHCO_3$, 0.02% NaN_3, pH 9.6 overnight at 37°C. Plates were washed with Tris-buffered saline (TBS) and blocked with Blocking solution (TBS containing 0.05% Tween20 and 1% gelatin) at 37°C for 2 hr. Sera were diluted at 1:1,600 in Blocking solution and pre-absorbed by immobilized GST protein at 4°C overnight. Then, 100 μl of the diluted sera was added to each well for overnight incubation at 4°C. Plates were washed with TBST (TBS containing 0.05% Tween20) and incubated with ALP-conjugated goat anti-human IgG Ab (Santa Cruz Biotechnology, CA) diluted at 1:1,000 in TBST (TBS containing 1% Tween20) for 2 hr at room temperature. After washing, bound WT1 IgG Ab was visualized using 50 μl of BCIP/NBT kit (Nacalai Tesque, Kyoto, Japan) for each well. Then, absorbance at 550 nm was measured using a microplate reader MTP-32 (Corona Electric, Ibaraki, Japan). All sera were examined in duplicate. The titers of WT1 IgG Ab were calculated by interpolation from the standard line which was constructed for each assay from the results of simultaneous ELISA assay using serial diluted WT1 6F-H2 Ab using ALP-conjugated goat anti-mouse IgG Ab (diluted at 1:1,000; Santa Cruz Biotechnology) as the second Ab. WT1 Ab titers in the sera that produced the absorbance at 550 nm equal to that produced by 0.1 μg/ml of WT1 monoclonal 6F-H2 (Dako Cytomation, Golstrup, Denmark) Ab was defined as a 1.0 WT1-reacting-unit (WRU) in the ELISA system. Thus, WT1 IgG Ab titers of sera were measured to be [(concentrations of 6F-H2 mAb (μg/ml) corresponding to the absorbance at 550 nm produced by the diluted sera on the standard line) × (ratio of serum dilution) × 10] WRU. When titers of WT1 IgG Ab were high and out of measurable range in the ELISA system, the sera were diluted with Blocking solution to measurable levels and reanalyzed to determine the titers of WT1 IgG Ab.

Western blot analysis

For detection of WT1 IgG Ab, sera were diluted at 1:1,000, reacted with immobilized recombinant GST protein (200 ng) at 4°C overnight, and then reacted at room temperature overnight with GST tagged, full length WT1 protein or one each of three WT1 fragment proteins (200 ng) that was transferred onto PVDF membrane after SDS-PAGE. WT1 IgG Ab captured by the protein was visualized by ALP-conjugated anti-human IgG Ab or ALP-conjugated anti-human IgG subclass-specific Ab using a BCIP/NBT kit (Nacalai Tesque).

For analysis of relative amount of subclasses of WT1 IgG Ab and total IgG, 5 μl of diluted serum (diluted at 1:10 with 2 × Laemieli's SDS sample buffer) were loaded onto SDS-PAGE gel and the serum proteins were transferred onto PVDF membrane. Then, the membrane was reacted with ALP-conjugated anti-human IgG subclass-specific Ab at room temperature overnight and the bound Ab was visualized by using a BCIP/NBT kit.

ALP-conjugated anti-human IgG Ab was purchased from Santa Cruz Biotechnology and used at the dilution of 1:1,000. ALP-conjugated anti-human IgG1 (#05-3322), IgG2 (#05-3522), IgG3 (#05-3622) and IgG4 (#05-3822) Ab were purchased from Zymed Laboratories (San Francisco, CA) and used at the dilution of 1:500. WT1 monoclonal 6F-H2 antibody against 180aa residues in the amino terminal region of WT1 protein (Dako Cytomation), WT1 polyclonal C-19 antibody against 19aa residues near the carboxy terminus of WT1 protein (Santa Cruz Biotechnology) and GST antibody (Santa Cruz Biotechnology) were used as a first antibody. WT1 IgG Ab detected in Western blot analysis was scored into three categories; positive (WT1 IgG Ab was detected as a band with strong or intermediate density), weakly positive (WT1 IgG Ab was detected as a band with weak density), and negative (WT1 IgG Ab was not detected).

Immunohistochemistry

Formalin-fixed tissue sections of 3-μm thickness were cut from each paraffin-block. After dewaxing with xylene and rehydration through a graded series of ethanol, the sections were antigen retrieved using Pascal apparatus (Dako Cytomation) in 10 mM citrate buffer (pH 6.0). These sections were reacted with WT1 C-19 Ab (diluted at 1:100, Santa Cruz Biotechnology) at 4°C overnight and then reacted with Envision kit/HRP (Dako Cytomation) at room temperature for 30 min. After treatment with 0.7% H_2O_2 so-

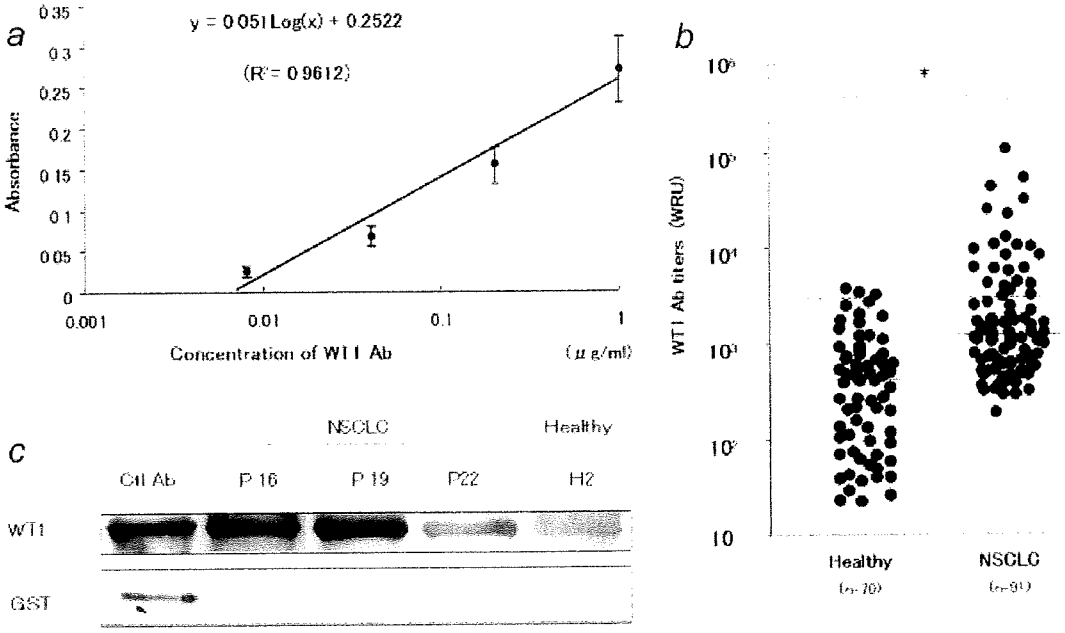

FIGURE 1 – Enhanced production of WT1 IgG Ab in NSCLC patients. (*a*) A representative standard line of the ELISA system for measurement of the titers of WT1 IgG Ab. The absorbance at 550 nm produced by serial dilution of WT1 monoclonal 6F-H2 Ab was measured by the ELISA system. The results are from four independent assays, and the mean ± SE is shown. WT1 Ab titer that produces the absorbance at 550 nm equal to that produced by 0.1 μg/ml of WT1 monoclonal 6F-H2 Ab in the ELISA system was defined as 1.0 WT1-reacting-unit (WRU). (*b*) Increased WT1 Ab titers in NSCLC patients. WT1 Ab titers were examined by the ELISA system in 91 NSCLC patients and 70 healthy individuals. Dotted line shows the cut-off level (2,910 WRU) of WT1 Ab titers, $*p < 0.05$. (*c*) Detection of WT1 IgG Ab by Western blot analysis in NSCLC patients. Western blot analysis was performed as described in "Material and Methods". As representative results, those from three NSCLC patients (P16, P19 and P22) and healthy individual (H2) are shown. WT1 monoclonal 6F-H2 Ab and GST Ab were used to show the positions of GST-WT1 protein and GST protein, respectively.

lution to reduce endogenous peroxidase activity, immunoreactive WT1 protein was visualized using DAB tablet (Wako, Osaka, Japan). The sections were then counterstained with hematoxylin.

Statistical analysis

The Welch's *t* test was used to calculate the difference between the titers of WT1 IgG Ab of NSCLC patients and those of healthy individuals. Statistical analysis for correlations between the titers of WT1 IgG Ab and the clinical parameters and was performed using Welch's *t* test or Kruskal–Wallis test. Statistical analysis for prognosis between NSCLC patients with or without elevated WT1 IgG Ab titers was performed by log-rank's test.

Results

Establishment of ELISA system for measurement of WT1 IgG Ab

Enzyme-linked immunosorbent assay (ELISA) system was established to measure the titers of WT1 IgG Ab (WT1 Ab titers) in the sera from NSCLC patients and healthy individuals. In the ELISA system, WT1 IgG Ab was captured by GST tagged, full length WT1 protein and visualized using ALP-conjugated anti-human IgG Ab. WT1 Ab titers were calculated by interpolation from the standard line, which was constructed from the results of simultaneous ELISA assay using serial diluted WT1 monoclonal 6F-H2 Ab. The absorbance at 550 nm produced by serially diluted WT1 monoclonal 6F-H2 Ab showed a linear plot ($R^2 = 0.9612$) against the concentrations of 6F-H2 Ab ranging from 0.008 to 1 μg/ml (Fig. 1*a*). WT1 Ab titers in the sera that produced the absorbance at 550 nm equal to that produced by 0.1 μg/ml of WT1 monoclonal 6F-H2 Ab was defined as a 1.0 WRU. Thus, WT1 IgG Ab titers of sera were measured to be [(concentrations of 6F-H2 mAb (μg/ml) corresponding to the absorbance at 550 nm produced by the diluted sera on the standard line) × (ratio of serum dilution) × 10] WRU. The standard line was reproducible with between-run coefficient of variation (CV) of 7.5% in 10 independent assays.

Elevation of WT1 IgG Ab in NSCLC patients

WT1 Ab titers (WRU) were examined in 91 NSCLC patients and 70 healthy individuals. WT1 IgG Ab was detected in all the samples examined (Fig. 1*b*). WT1 Ab titers ranged from 10 to 3,664 (median 392) and from 183 to 104,940 (median 1,135) WRU in healthy individuals and NSCLC patients, respectively. Therefore, WT1 Ab titers were significantly ($p < 0.05$) higher in NSCLC patients than in healthy individuals. When the cut-off level of WT1 Ab titers was fixed at 2,910 WRU, which was mean + 3SD of WT1 Ab titers in healthy individuals, 24 (26.4%) of 91 NSCLC patients had WT1 Ab over the cut-off level.

To confirm the presence of WT1 IgG Ab in sera from NSCLC patients and healthy individuals, sera of randomly selected 31 NSCLC patients and 27 healthy individuals were reacted with immobilized recombinant GST protein and then examined for WT1 IgG Ab by Western blot analysis using GST-WT1 protein as an antigen. WT1 IgG Ab was detected in all of the 31 NSCLC patients and 27 healthy individuals examined (Fig. 1*c*, upper panels). Furthermore, to confirm that the bands detected did not result from the reaction of GST portion of GST-WT1 protein with antibodies against GST in the patients' sera, Western blot analysis was performed using the sera which was pre-reacted with immobilized GST protein and purified GST protein as an antigen. As expected, sera of the patients and healthy individuals did not react with GST protein (Fig. 1*c*, lower panels). These results showed that Western blot analysis used here could specifically detect WT1 IgG Ab.

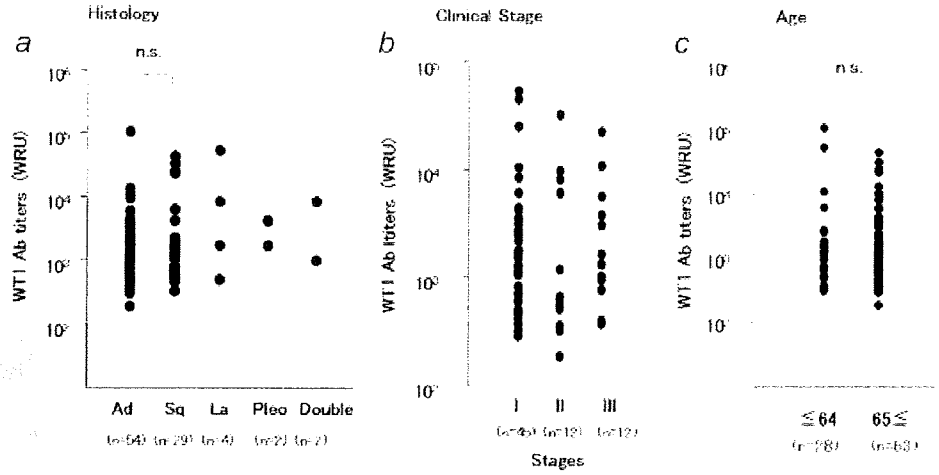

FIGURE 2 – No correlation between WT1 Ab titers and clinical parameters of NSCLC. Correlations between WT1 Ab titers and clinical parameters of NSCLC, histology (*a*), clinical stages (*b*) and age (*c*) are shown. n.s., Not significant.

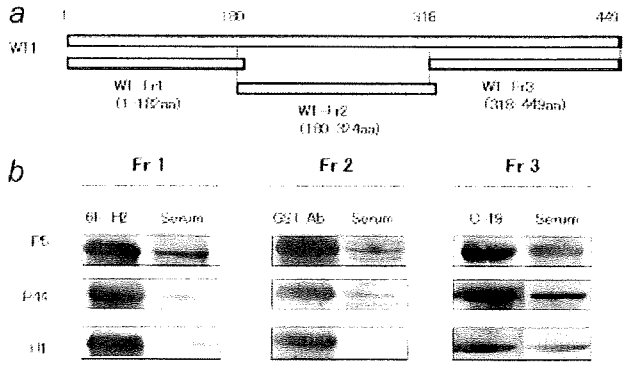

FIGURE 3 – Epitope distribution of WT1 IgG Ab. (*a*) Schema of WT1 fragment proteins. Recombinant WT1 fragment proteins were expressed in bacterial hosts. (*b*) Western blot analysis for epitope distribution of WT1 IgG Ab. Western blot analysis was performed. WT1 antibodies, 6F-H2 monoclonal Ab against 180 aa residues at the amino terminus of WT1 protein and C-19 polyclonal Ab against 19 aa residues near the carboxy terminus were used as positive control antibodies recognizing WT-Fr1 and WT-Fr3, respectively. Because WT1 antibody recognizing WT-Fr2 was not available, GST antibody was used to show the band responsible for WT-Fr2 with GST tag. Representative results of NSCLC patients (P5 and P44) and a healthy individual (H1) are shown.

No correlation between WT1 Ab titers and clinical parameters in NSCLC patients

Whether or not WT1 Ab titers were correlated with clinical parameters was examined in NSCLC patients. As shown in Figure 2, no correlation was found between WT1 Ab titers and clinical parameters such as histology, clinical stages and age.

Epitope distribution of WT1 IgG Ab in NSCLC patients and healthy individuals

Epitope distribution of WT1 IgG Ab was examined in the 31 NSCLC patients and 27 healthy individuals by Western blot analysis using three purified, recombinant WT1 fragment proteins, WT-Fr1 (1–182aa), WT-Fr2 (180–324aa) and WT-Fr3 (318–449aa) as antigens (Fig. 3*a*). Sera from 30 (96.8%) of 31 NSCLC patients and 24 (88.9%) of 27 healthy individuals examined recognized two or three WT1 fragment proteins (Fig. 3*b*). These results indicated the presence of multiple antigenic epitopes within WT1 protein.

Dominant subclass of WT1 IgG Ab is IgG2

To examine whether humoral immune responses against WT1 protein were Th1- or Th2- type, subclasses of WT1 IgG Ab against WT-Fr3 protein, which was recognized by all of the sera examined, were examined by Western blot analysis in the 31 NSCLC patients and the 27 healthy individuals (Fig. 4). IgG2 was a dominant subclass of WT1 Ab in all of the patients and healthy individuals examined (Fig. 4*a*, upper panels). To confirm that this IgG2 dominance did not result from the reflection of the dominance of total IgG2 subclass, subclasses of total IgG were simultaneously determined (Fig. 4*a*, lower panels). Differently from the IgG2 dominance of WT1 IgG Ab, the dominant subclass of total IgG was IgG1. These results showed that dominant subclass of WT1 IgG Ab was IgG2. In NSCLC patients, positivity (see "Material and Methods") of WT1 IgG1, IgG2, IgG3 and IgG4 subclass Ab were 22.6% (7 of 31), 64.5% (20 of 31), 19.4% (6 of 31) and 12.9% (4 of 31), respectively (Figs. 4*a*, 4*b*). In healthy individuals, positivity of WT1 IgG1, IgG2, IgG3 and IgG4 subclass Ab were 22.2% (6 of 27), 77.8% (21 of 27) , 29.6% (8 of 27) and 29.6% (8 of 27), respectively.

To confirm the semiquantitative nature of the Western blot analysis used here, it was performed by using WT-Fr3 protein as an antigen and serially diluted serum from a NSCLC patient (P4). As shown in Fig. 4*c*, the band density of IgG2 WT1 Ab, which was dominantly contained in the serum, decreased as the serum was diluted at the ratio of 1:200, 1:600 and 1:1,800, confirming that the Western blot analysis used here could semi-quantitatively detect WT1 IgG Ab.

Therefore, production of Th1-type, IgG2 WT1 Ab was enhanced in NSCLC patients, indicating that Th1-type humoral immune responses against WT1 protein were elicited in NSCLC patients.

WT1 Ab as a biomarker for detection of NSCLC

Positivity of WT1 Ab was compared with that of currently available tumor markers, CEA and CYFRA, in NSCLC patients. Clinical data of CEA and CYFRA were available for 70 (44 on stage I, 13 on stage II and 13 on stage III) and 59 patients (36 on stage I, 12 on stage II and 11 on stage III) with NSCLC, respectively. As shown in Figure 5, WT1 Ab titers did not correlate with serum levels of CEA (Fig. 5*a*) and CYFRA (Fig. 5*b*). Positive detection rate for WT1 Ab, CEA and CYFRA was 25.0 (11 of 44), 13.6 (6 of 44) and 11.1% (4 of 36) in stage I NSCLC patients; 30.8 (4 of 13), 23.1 (3 of 13) and 16.7% (2 of 12) in stage II patients and 38.5 (5 of 13), 46.2 (6 of 13) and 18.2% (2 of 11) in stage III patients, respectively (Fig. 5*c*). Because positive detec-

tion rate of WT1 Ab was 25.0%, which was higher than that of either CEA or CYFRA, in stage I NSCLC patients, it may be a useful marker for early detection of NSCLC.

When WT1 Ab was combined with CEA or CYFRA for detection of NSCLC, positive detection rates increased from 25.0 to 34.1 and 31.8%, respectively, in stage I and from 38.4 to 69.2 and 46.1%, respectively, in stage III, but not changed in stage II (Fig. 5*c*). Thus, WT1 Ab is useful for sensitive detection of NSCLC in combination with CEA or CYFRA.

Overexpression of WT1 protein in early stage NSCLC

To confirm the expression of WT1 protein in early stage NSCLC, the expression of WT1 protein was examined by immunohistochemistry in 41 patients with stage I NSCLC. WT1 expression in cancer cells was scored into the following three categories: positive, weakly positive and negative staining meant strong, slightly stronger and similar one of lung cancer cells, respectively, compared with that of the alveolar epithelial cells of lung. In positive or weakly positive cases, WT1 protein was dominantly detected in the cytoplasm of lung cancer cells. WT1 protein expression in lung cancer cells was positive in 30 (73.2%), weakly positive in 7 (17.1%), and negative in the remaining 4 (9.8%), of 41 NSCLC patients (Fig. 5*d*). Thus, WT1 protein was overexpressed in 90.3% (37 of 41) of stage I NSCLC patients examined.

Elevation of WT1 Ab is associated with favorable prognosis in NSCLC patients

To examine whether or not enhanced humoral immune responses against WT1 were associated with lower relapse rates in patients with NSCLC, DFS rates were analyzed between two groups of NSCLC patients whose follow-up data after surgery were available: 20 patients with elevated WT1 Ab titers (52,110–3,514; median 8,777 WRU) and 59 patients without elevated WT1 Ab titers (2,648–183; median 655 WRU). In patients with elevated WT1 Ab titers, 1-, 2- and 3-year DFS rates of the patients were 100, 94.7 and 94.7%, respectively. In contrast, in patients without elevated WT1 Ab titers, 1-, 2- and 3-year DFS rates were 88.0, 82.8 and 77.4%, respectively. Kaplan–Meier curve and log rank's test showed that patients with elevated WT1 Ab titers had significantly ($p = 0.002$) longer DFS than those without them (Fig. 6). These results indicated that enhancement of humoral immune responses against WT1 was associated with favorable prognosis in patients with NSCLC.

Discussion

In the present study, we showed that WT1 IgG Ab was produced in all of the 91 NSCLC patients and 70 healthy individuals and that 26.4% of the NSCLC patients had WT1 IgG Ab titers over the cut-off level which was mean + 3SD of those of healthy individuals. These findings showed two aspects of WT1 specific immune responses in NSCLC patients. One was that, in consistence with our previous reports on patients with leukemia and MDS,[17,18] humoral immune responses were also elicited against cancer-derived WT1 protein in patients with NSCLC. The elevation of WT1 Ab titers were found even in stage IA NSCLC in which tumor size was less than 3 cm, indicating that the immune system could recognize cancer-derived WT1 protein and respond to it when its amount was still small. Another was the difference in the immune responses against WT1 protein in individual NSCLC patients. No differences were observed in clinical param-

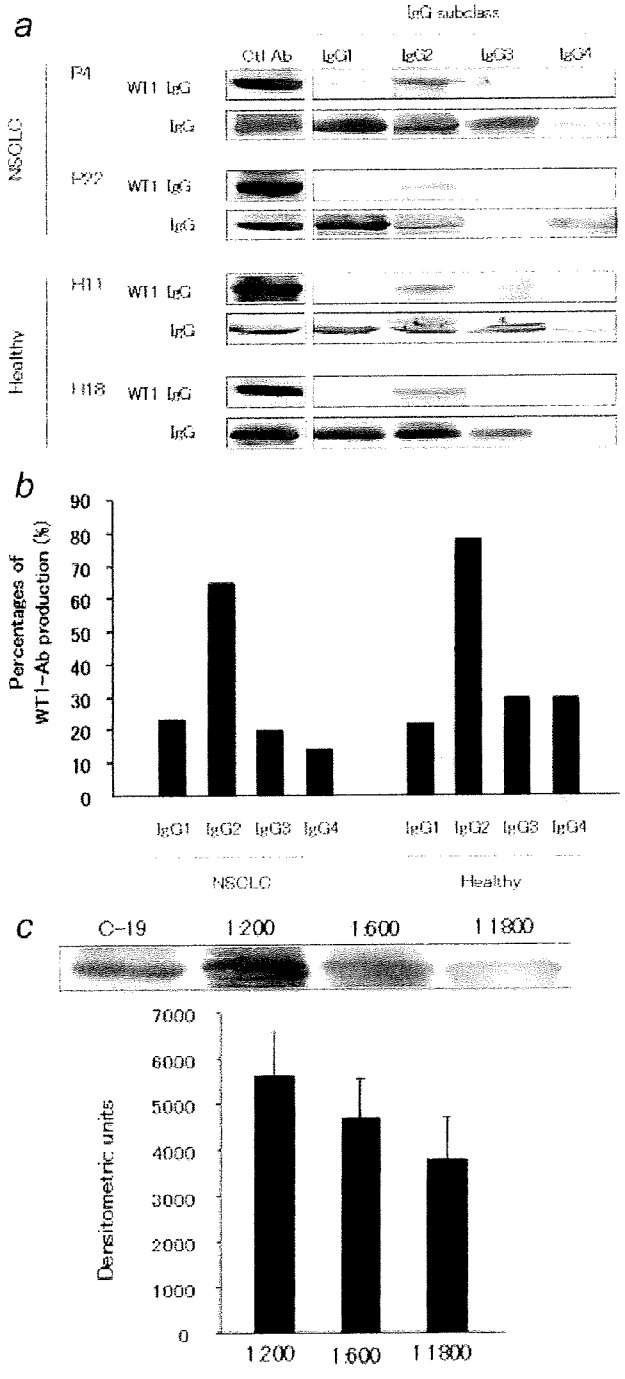

FIGURE 4 – Subclass distribution of WT1 IgG Ab. Recombinant WT1 fragment protein (WT-Fr3, approximately 200 ng/lane) was subjected to Western blot analysis using sera from NSCLC patients and healthy individuals as first antibodies. Membrane bound WT1 IgG Ab was visualized using IgG subclass-specific second Ab. (*a*) Representative results of Western blot analysis for WT1 IgG Ab and IgG subclasses in NSCLC patients (P4 and P22) and healthy individuals (H11 and H18). Results of WT1 IgG Ab (upper panels) and total IgG (lower panels) subclasses were displayed in pairs for each patient and healthy individual. WT1 polyclonal C-19 Ab and IgG Ab were used to confirm the positions of the bands responsible for WT1 IgG Ab and IgG, respectively. (*b*) Positive rate of each subclass of WT1 IgG Ab produced in NSCLC patients and healthy individuals is graphically shown. (*c*) Semiquantitative nature of the Western blot analysis. Western blot analysis was performed for detecting IgG2 WT1 Ab, which was dominantly contained in the serum, by using WT1-Fr3 protein as an antigen and serially diluted serum from a NSCLC patient (P4) (upper). To confirm the band of WT1 IgG Ab, polyclonal WT1 Ab C-19 was used. The band density obtained from the diluted serum is graphically shown as the mean (columns) and SD (bars) of four independent experiments (lower).

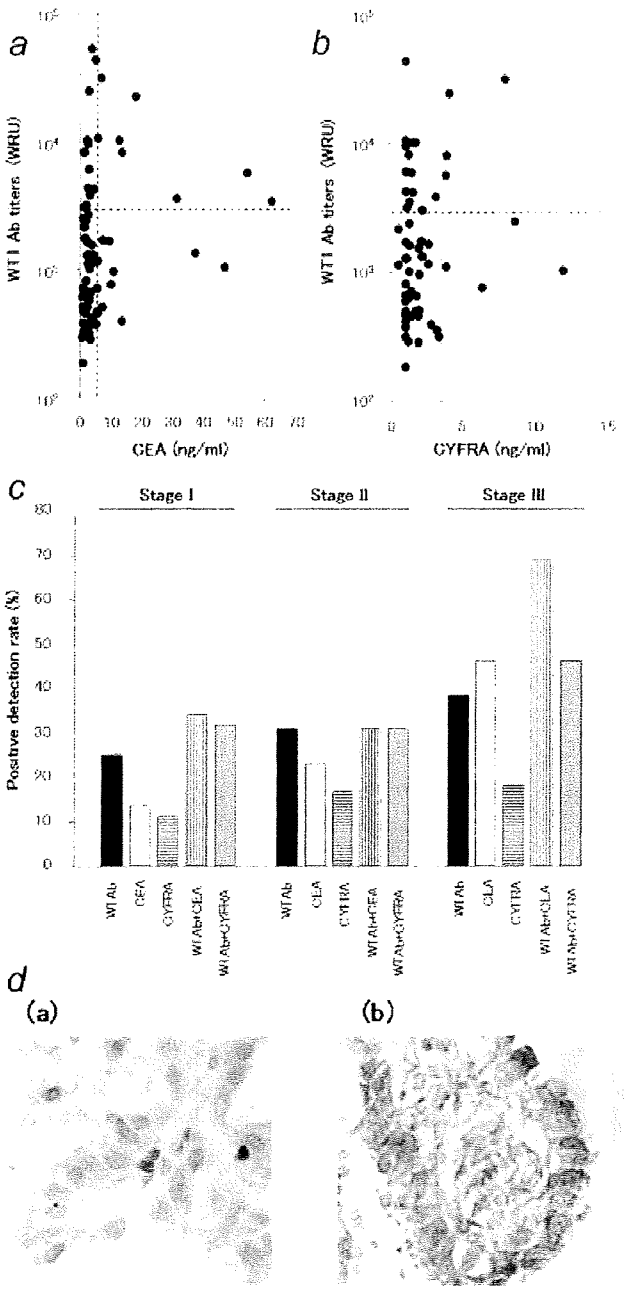

FIGURE 5 – WT1 Ab level as a marker for detection of NSCLC. No correlation between WT1 Ab levels and levels of current NSCLC tumor marker, (*a*) CEA (n = 70) or (*b*) CYFRA (n = 59). Dotted line indicates the cut-off level for each marker. (*c*) Positive detection rate for NSCLC. (*d*) Overexpression of WT1 protein in stage I NSCLC. Expression of WT1 protein was examined by immunohistochemistry in stage I NSCLC. (*a*, *b*) Representative results of different cases are shown. WT1 protein is detected in brown.

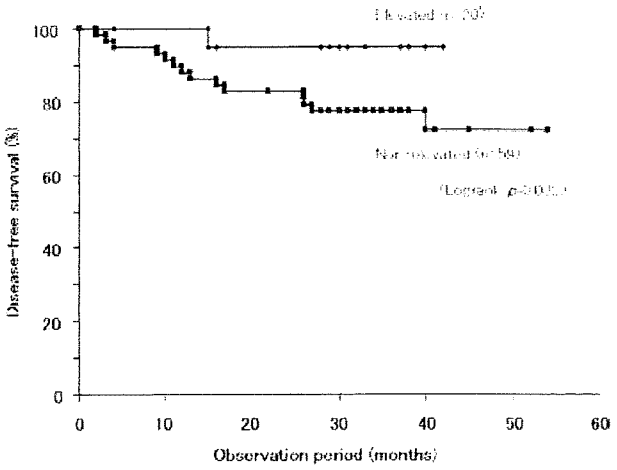

FIGURE 6 – Kaplan–Meier curves for disease-free survival in 79 NSCLC patients. The results from NSCLC patients with elevated WT1 IgG Ab titers (elevated, n = 20) and without them (nonelevated, n = 59) are shown.

eters such as histology, clinical stages and age among NSCLC patients with or without elevated WT1 Ab titers. Thus, the reason why a part of NSCLC patients highly produced WT1 Ab remains undetermined.

There is a great need to develop novel biomarkers for early detection of NSCLC. In the present study, we showed that positive detection rate of WT1 Ab was higher than that of CEA or CYFRA in stages I and II NSCLC. One reason for it should be the difference in the substances measured in these assays. Because the currently available cancer biomarkers such as CEA and CYFRA are based on the measurement of the substances released into blood from cancer cells, detection of such substances may be difficult until cancer becomes advanced and releases considerable amount of the substances. In contrast, measurement of WT1 Ab is an assay of antigen-specific humoral immune responses. Even if early cancer releases small amount of tumor antigens, host immune system is considered to be able to recognize small amount of antigens and respond to them. Through this process, a signal with antigenic tumor protein is biologically amplified to the detectable level.[19] Furthermore, because WT1 Ab was an independent tumor marker that was not correlated with serum levels of CEA and CYFRA, combination of WT1 Ab with CEA or CYFRA increased the positive detection rates for NSCLC. Taken together, these results indicated that WT1 Ab was a useful serum marker for early detection of NSCLC.

Helper T cells are central regulators of both humoral and cellular immune responses.[20] Th1 cells are primarily responsible for activating and regulating the development and persistence of cytotoxic T lymphocyte. In addition, Th1 cells activate antigen-presenting cells and induce the production of Th1 type antibodies (IgG1, 2 and 3), whereas Th2 cells promote that of Th2 type one (IgG4). In the present study, we analyzed the subclass of WT1 IgG Ab and showed that dominant subclass of WT1 IgG Ab was Th1-type IgG2 in NSCLC patients, indicating activation of Th1 type WT1-specific immune responses. These results might indicate that WT1-specific $CD8^+$ cytotoxic T lymphocyte (CTL) responses were more activated in NSCLC patients with elevated WT1 Ab titers compared with those without them. Interestingly, high titers of WT1 IgG Ab were associated with longer DFS in NSCLC patients. This may be explained by the activated WT1-specific $CD8^+$ CTL responses in NSCLC patients with elevated WT1 Ab titers. Another possible explanation is a direct cytotoxic effect of WT1-specific $CD4^+$ T lymphocytes on NSCLC cells. Recently, direct recognition and lysis of leukemia cells by WT1-specific $CD4^+$ T lymphocytes in an HLA class II-restricted manner were reported.[21] Because elevated WT1 Ab titers were considered to be associated with activation of WT1-specific $CD4^+$ T lymphocytes and because HLA class II molecules were expressed in NSCLC cells,[22] it was possible that WT1-specific $CD4^+$ T lymphocytes exert their cytotoxic activities against NSCLC. These findings and our results presented here indicated that WT1-specific immune responses played an important role in anti-tumor immu-

nity against NSCLC and that WT1 IgG Ab was a good marker for prognostic prediction of NSCLC.

Although many reports show the production of antibodies against autoantigens in cancer patients,[23–25] that of these antibodies in healthy individuals remains unclear. This study showed that WT1 IgG Ab was produced in all of the healthy individuals examined. The titers of WT1 IgG Ab in these individuals were low and dominant subclass of WT1 IgG Ab was Th1-type IgG2. Thus, Th1-type humoral immune responses were weakly elicited in healthy individuals. Moreover, our previous report showed that WT1-specific CTLs exist at a percentage of 0.04 ± 0.02% of $CD8^+$ T-cells in peripheral blood mononuclear cells of five healthy volunteers.[26] The frequency seems to be higher than that of CTLs against other antigens such as gp100 or Tyrosinase.[27] These results indicated that WT1 protein elicited both humoral and cellular immune responses in healthy individuals, indicating its high immunogenecity. As for the source of WT1 antigen in healthy individuals, one possible source of WT1 antigen is normal WT1-expressing organs such as urogenital systems and mesothelium.[28] Although these organs express WT1 protein at high levels, no injury was observed in the patients vaccinated with WT1 peptide in clinical trials,[29] suggesting that the normal WT1-expressing organs are protected from WT1-specific immune responses by unknown mechanism. Another source may be undetectable tumors expressing WT1. It is considered that tumors develop in healthy individuals but are eliminated by host immune surveillance system before tumors grow to detectable levels.[30] Because WT1 protein is highly immunogenic, WT1-specific immune responses may function as one of immune surveillance system against cancer in healthy individuals.

Acknowledgements

The authors thank Dr. Yoshinori Iwatani (Department of Biomedical Informatics, Osaka University Graduate School of Medicine) for his advice on ELISA.

References

1. Schrump DS, Altorki NK, Henschke CL, Carter D, Turrisi AT, Gutierrez ME. Cancer: principles and practice of oncology, 7th edn. Philadelphia: Lippincott Williams and Wilkins, 2005;753–810.
2. Bastarrika G, García-Velloso MJ, Lozano MD, Montes U, Torre W, Spiteri N, Campo A, Seijo L, Alcaide AB, Pueyo J, Cano D, Vivas I, et al. Early lung cancer detection using spiral computed tomography and positron emission tomography. Am J Respir Crit Care Med 2005;171:1378–83.
3. Mulshine JL. Clinical issues in the management of early lung cancer. Clin Cancer Res 2005;11:4993s–8s.
4. Burt RW, Ratcliffe JG, Stack BH, Cuthbert J, Kennedy RS, Corker CS, Franchimont P, Spilg WG, Stimson WH. Serum biochemical markers in lung cancer. Br J Cancer 1978;37:714–7.
5. Boddy JJ, Sculier JP, Raymakers N, Paesmans M, Ravez P, Libert P, Richez M, Dabouis G, Lacroix H, Bureau G, Thiriaux J, Lecomte J, et al. Evaluation of squamous cell carcinoma antigen as a new marker for lung cancer. Cancer 1990;65:1552–6.
6. Call KM, Glaser T, Ito CY, Buckler AJ, Pelletier J, Haber DA, Rose EA, Kral A, Yeger H, Lewis WH, Jones C, Housman DE. Isolation and characterization of a zinc finger polypeptide gene at the human chromosome 11 Wilms' tumor locus. Cell 1990;60:509–20.
7. Inoue K, Sugiyama H, Ogawa H, Nakagawa M, Yamagami T, Miwa H, Kita K, Hiraoka A, Masaoka T, Nasu K, Kyo T, Dohy H, et al. WT1 as a new prognostic factor and a new marker for the detection of minimal residual disease in acute leukemia. Blood 1994;84:3071–9.
8. Oji Y, Miyoshi S, Maeda H, Hayashi S, Tamaki H, Nakatsuka S, Yao M, Takahashi E, Nakano Y, Hirabayashi H, Shintani Y, Oka Y, et al. Overexpression of the Wilms' tumor gene WT1 in *de novo* lung cancers. Int J Cancer 2002;100:297–303.
9. Oji Y, Miyoshi S, Takahashi E, Koga S, Nakano Y, Shintani Y, Hirabayashi H, Matsumura A, Iuchi K, Ito K, Kishimoto Y, Tsuboi A, et al. Absence of mutations in the Wilms' tumor gene wt1 in *de novo* non-small cell lung cancers. Neoplasma 2004;51:17–20.
10. Nakatsuka SI, Oji Y, Horiuchi T, Kanda T, Kitagawa M, Takeuchi T, Kawano K, Kuwae Y, Yamauchi A, Okumura M, Kitamura Y, Oka Y, et al. Immunohistrochemical detection of WT1 protein in a variety of cancer cells. Mod Pathol 2006;19:804–14.
11. Oji Y, Yano M, Nakano Y, Abeno S, Nakatsuka S, Ikeba A, Yasuda T, Fujiwara Y, Takiguchi S, Yamamoto H, Fujita S, Kanato K, et al. Overexpression of the Wilms' tumor gene WT1 in esophageal cancer. Anticancer Res 2004;24:3103–8.
12. Oji Y, Yamamoto H, Nomura M, Nakano Y, Ikeba A, Nakatsuka S, Abeno S, Kiyotoh E, Jomgeow T, Sekimoto M, Nezu R, Yoshikawa Y, et al. Overexpression of the Wilms' tumor gene WT1 in colorectal adenocarcinoma. Cancer Sci 2003;94:712–7.
13. Oji Y, Nakamori S, Fujikawa M, Nakatsuka S, Yokota A, Tatsumi N, Abeno S, Ikeba A, Takashima S, Tsujie M, Yamamoto H, Sakon M, et al. Overexpression of the Wilms' tumor gene WT1 in pancreatic ductal adenocarcinoma. Cancer Sci 2004;95:583–7.
14. Sugiyama H. Wilms' tumor gene WT1: its oncogenic function and clinical application. Int J Hematol 2001;73:177–87.
15. Ito K, Oji Y, Tatsumi N, Shimizu S, Kanai Y, Nakazawa T, Asada M, Jomgeow T, Aoyagi S, Nakano Y, Tamaki H, Sakaguchi N, et al. Antiapoptotic function of 17AA(+)WT1 (Wilms' tumor gene) isoforms on the intrinsic apoptosis pathway. Oncogene 2006;25:4217–29.
16. Jomgeow T, Oji Y, Tsuiji N, Ikeda Y, Ito K, Tsuda A, Nakazawa T, Tatsumi N, Sakaguchi N, Takashima S, Shirakata T, Nishida S, et al. Wilms' tumor gene WT1 17AA(-)/KTS(-) isoform induces morphological changes and promotes cell migration and invasion in vitro. Cancer Sci 2006;97:259–70.
17. Elisseeva OA, Oka Y, Tsuboi A, Ogata K, Wu F, Kim EH, Soma T, Tamaki H, Kawakami M, Oji Y, Hosen N, Kubota T, et al. Humoral immune responses against Wilms' tumor gene WT1 product in patients with hematopoietic malignancies. Blood 2002;99:3272–9.
18. Wu F, Oka Y, Tsuboi A, Elisseeva OA, Ogata K, Nakajima H, Fujiki F, Masuda T, Murakami M, Yoshihara S, Ikegame K, Hosen N, et al. Th1-biased humoral immune responses against Wilms tumor gene WT1 product in the patients with hematopoietic malignancies. Leukemia 2005;19:268–74.
19. Hanash S. Harnessing immunity for cancer marker discovery. Nat Biotechnol 2003;21:37–8.
20. Knutson KL, Disis ML. Tumor antigen-specific T helper cells in cancer immunity and immunotherapy. Cancer Immunol Immnother 2005;54:721–8.
21. Guo Y, Niiya H, Azuma T, Uchida N, Yakushijin Y, Sakai I, Hato T, Takahashi M, Senju S, Nishimura Y, Yasukawa M. Direct recognition and lysis of leukemia cells by WT1-specific $CD4^+$ T lymphocytes in an HLA class II-restricted manner. Blood 2005;106:1415–8.
22. Redondo M, Ruiz-Cabello F, Concha A, Hortas ML, Serrano A, Morell M, Garrido F. Differential expression of MHC class II genes in lung tumour cell lines. Eur J Immunogenet 1998;25:385–91.
23. Cho-Chung YS. Autoantibody biomarkers in the detection of cancer. Biochim Biophys Acta 2006;1762:587–91.
24. Brichory F, Beer D, Le Naour F, Giordano T, Hanash S. Proteomics-based identification of protein gene product 9.5 as a tumor antigen that induces a humoral immune response in lung cancer. Cancer Res 2001;61:7908–12.
25. He P, Naka T, Serada S, Fujimoto M, Tanaka T, Hashimoto S, Shima Y, Yamadori T, Suzuki H, Hirashima T, Matsui K, Shiono H, et al. Proteomics-based identification of alpha-enolase as a tumor antigen in non-small lung cancer. Cancer Sci 2007;98:1234–40.
26. Kawakami M, Oka Y, Tsuboi A, Harada Y, Elisseeva OA, Furukawa Y, Tsukaguchi M, Shirakata T, Nishida S, Nakajima H, Morita S, Sakamoto J, et al. Clinical and immunologic responses to very low-dose vaccination with WT1 peptide (5microgram/body) in a patient with chronic myelomonocytic leukemia. Int J Hematol 2007;85:426–9.
27. Mortarini R, Piris A, Maurichi A, Molla A, Bersani I, Bono A, Bartoli C, Santinami M, Lombardo C, Ravagnani F, Cascinelli N, Parmiani G, et al. Lack of terminally differentiated tumor-specific $CD8^+$ T cells at tumor site in spite of antitumor immunity to self-antigens in human metastatic melanoma. Cancer Res 2003;63:2535–45.
28. Menke AL, van der Eb AJ, Jochemsen AG. The Wilms' tumor 1 gene: oncogene or tumor suppressor gene? Int Rev Cytol 1998;181:151–212.
29. Oka Y, Tsuboi A, Taguchi T, Osaki T, Kyo T, Nakajima H, Elisseeva OA, Oji Y, Kawakami M, Ikegame K, Hosen N, Yoshihara S, et al. Induction of WT1 (Wilms' tumor gene)-specific cytotoxic T lymphocytes by WT1 peptide vaccine and the resultant cancer regression. Proc Natl Acad Sci USA 2004;101:13885–90.
30. Dunn GP, Bruce AT, Ikeda H, Old LJ, Schreiber RD. Cancer immunoediting: from immunosurveillance to tumor escape. Nat Immunol 2002;3:991–8.

Cancer Science
The official journal of the Japanese Cancer Association JCA

A Quantitative trait locus responsible for inducing B-cell lymphoblastic lymphoma is a hotspot for microsatellite instability

Richard H. Kaszynski,[1] Shinya Akatsuka,[2] Takuya Hiratsuka,[3] Guang Jin,[4] Munetaka Ozeki,[1] Tomoko Okuno,[1] Takuro Nakamura,[4] Toshiaki Manabe,[5] Tetsuya Takakuwa,[6] Hiroshi Hiai,[7] Shinya Toyokuni,[2] Keiji Tamaki[1] and Tatsuaki Tsuruyama[1,8]

[1]Department of Forensic Medicine and Molecular Pathology, Graduate School of Medicine, Kyoto University, Kyoto; [2]Department of Pathology and Biological Responses, Graduate School of Medicine, Nagoya University, Nagoya; [3]Department of Pathology, Saisei-kai Noe Hospital, Osaka; [4]Laboratory of Carcinogenesis, Cancer Institute, Tokyo; [5]Department of Diagnostic Pathology, Graduate School of Medicine, Kyoto University, Kyoto; [6]Department of Human Health Science, Graduate School of Medicine, Kyoto University, Kyoto; [7]Shiga Medical Center Research Institute, Shiga, Japan

(Received September 24, 2009/Revised November 2, 2009/Accepted November 4, 2009)

While the molecular mechanisms underlying microsatellite instability (MSI) have been exhaustively investigated, identifying the patterns of MSI distribution within diverse cancer genomes has remained an elusive issue. In the present study, we conducted genome-wide MSI screening in B-cell lymphoblastic lymphomas (B-LBL) which spontaneously develop in the SL/Kh strain of mice. Tumor samples harvested from 16 mice were investigated using a framework map consisting of 150 microsatellite markers spaced at increments of roughly 0.5–3.0 centimorgans, spanning the entirety of mouse chromosomes (mus musculus chromosomes [MMU]) 3–6. MMU3 contains a quantitative trait locus (QTL), *Bomb1* (bone marrow pre-B1), known to induce an aberrant expansion of pre-B cells in bone marrow prior to the onset of B-LBL in SL/Kh mice. The remaining chromosomes were selected on the basis of those most closely resembling MMU3 in terms of total estimated length (maximum variance 10 Mb). MSI was confirmed at 2≤ markers in DNA derived from tumor tissues in 15 SL/Kh mice (93.7%), while healthy splenic DNA samples screened in parallel were consistently negative for MSI. The overall MSI incidence was significantly higher on MMU3 compared with MMU4–6 ($P = 0.031$). Additionally, by applying spatial point pattern analysis combined with a 1-D version of Ripley's *K*-function, we successfully demonstrated the predilection of MSI-susceptible loci to structure a massive cluster within the *Bomb1* locus. Our study is the first to suggest that a QTL concomitantly serves as a hotspot for MSI-susceptible loci and sheds new light on somatic cancer genetics. (*Cancer Sci* 2010; 101: 800–805)

B-cell lymphoblastic lymphomas (B-LBL) are a prototypic high-grade neoplasm composed of immature lymphocytes that demonstrate lymphoblastic morphology and express pan-early B-cell markers.[1–4] As with humans, B-LBL are a relatively rare hematopoietic malignancy in mice.[5]

In our previous studies, we reported on the SL/Kh strain, which is a highly unique cancer model that spontaneously develops lymphomas recapitulating the human entity B-LBL at a high incidence (>90%) and relatively short latency (≤6 months of age).[6–8] An exclusive phenotype associated with the SL/Kh strain is the transient polyclonal expansion of $BP\text{-}1^{+}B220^{+}$ pre B cells in prelymphoma-stage bone marrow (BM), which heralds the development of overt B-LBL.[9,10] A highly significant quantitative trait locus (QTL) responsible for this aberrant expansion of pre-B cells in SL/Kh BM was mapped down to the distal segment of mus musculus chromosome (MMU)3, between 55 centimorgans (cM) (D3Mit300) and 78.5 cM (D3Mit45), and was subsequently termed *Bomb1* (BM pre-B1). In our most recent study, we confirmed that *Bomb1* is in fact responsible for this precursor lesion to B-LBL by constructing a speed congenic strain NFS.SL/Kh–*Bomb1*, in which the *Bomb1* segment of the SL/Kh mouse is introgressed into the genomic canvas of NFS/N mice.[11]

In the course of genotyping this QTL, we encountered a genetic lesion referred to as microsatellite instability (MSI) at high frequencies within the *Bomb1* locus of the SL/Kh lymphoma genome. MSI specificity in tumor cells was first reported in sporadic colorectal tumors,[12,13] and is now widely recognized as a hallmark of defective post-replicative DNA mismatch repair (MMR).[14–16] Since its initial discovery, the presence and frequency of MSI has been exhaustively investigated in a wide spectrum of cancers;[17–25] however, identifying the patterns of MSI distribution within these genomes has never been the object of a thorough examination. Therefore, based on our preliminary findings, we asked ourselves whether the QTL concomitantly serves as a hotspot for MSI-susceptible loci.

To answer this question, we applied a framework map consisting of 150 strategically positioned microsatellites markers at increments of 0.5 to 3 cM to analyze the spatial distribution patterns of MSI within the SL/Kh B-LBL genome. The expected microsatellite mutation rate per locus was a factor considered in erecting the framework map. Hanford *et al.* show that microsatellite mutations accumulate at defined rates per locus per generation in both MMR-proficient (HT-1080, fibrosarcoma) and -deficient (H6, colorectal carcinoma; LoVo, metastatic adenocarcinoma) cancer cell lines.[26] Based on these findings, we reasoned that the overall MSI ratio on chromosomes of equivalent size should be roughly comparable, and selected MMU4, MMU5, and MMU6 as references for our genome-wide assessment after confirming that they display the closest resemblance to MMU3 in terms of total estimated length (maximum variance 10 Mb), as determined via data retrieved from the Mouse Genome Database (MGD).[27] In the present study, we show that the *Bomb1* locus demonstrates markedly increased susceptibility towards MSI accumulation compared with other randomly distributed loci in the SL/Kh lymphoma genome.

Materials and Methods

Animal experiments. Animal experiments were performed with expressed written consent from the Ethics Committee for Animal Experiments, Graduate School of Medicine, Kyoto University (Kyoto, Japan). The origin and genetic properties of SL/Kh and congenic NFS.SL/Kh–*Bomb1* mice have been described

[8]To whom correspondence should be addressed.
E-mail: tsuruyam@kuhp.kyoto-u.ac.jp

doi: 10.1111/j.1349-7006.2009.01437.x

elsewhere.[7,8,11] NFS/N mice have been maintained by sister–brother mating for over 100 generations at the Institute of Laboratory Animals, Kyoto University; SL/Kh mice have been deposited into the National Bio-Resource Project (http://www.anim.med.kyoto-u.ac.jp/nbr/home.htm) at RIKEN (Tsukuba, Japan).

Marker selection. A framework map consisting of 150 polymorphic, microsatellite DNA markers was constructed. Markers were selected to assess the distribution patterns of loci with observed MSI (MSI-susceptible loci) in the SL/Kh genome using MMU3–6 as representative chromosomes. Markers and sequence information for primer pairs were retrieved from the MGD.[27] An intermarker genomic proportion criterion was established to space individual markers at increments of roughly 0.5–3 cM. On sporadic occasions, markers were unavailable to fit within the defined criterion (maximum variance 6.5 cM; MMU6). The markers adopted in this study, along with their chromosomal positions, are provided in the supporting Data S1.

Sample selection. Screening for MSI was performed on B-LBL tissues harvested from 16 SL/Kh mice. Used as the control, DNA isolated from the spleen of SL/Kh mice, the BM of NFS/N, and the congenic strain NFS.SL/Kh–*Bomb1*, were screened in parallel for this study. NFS/N mice are a well-established inbred strain and were selected on the basis of lacking the genetic information of an endogenous ecotropic murine leukemia virus[28] and for having a reportedly low spontaneous incidence of lymphomas and other neoplastic growths.[29] Splenic tissue was selected for the SL/Kh strain on the basis of being a highly vascular lymphoid organ responsible for producing lymphocytes and for having an inherent sensitivity to hematopoietic disorders, such as leukemia and lymphoma. In contrast, BM was selected for the congenic strain, given that the introgressed SL/Kh *Bomb1* segment gives rise to an expansion of pre-B cells in BM resembling the precursor lesion to overt lymphoma development in SL/Kh mice.[11] Additionally, the NFS/N strain serves as the foundation in which the congenic mouse was developed upon, and therefore, BM was similarly adopted as a control for the NFS/N strain.

DNA extraction and isolation. Genomic DNA was extracted from the spleen, lymphoma, and BM using a QIAamp minikit (Qiagen, Valencia, CA, USA) according to the manufacturer's recommended protocol. Following extraction and isolation, DNA obtained from these methods were subjected to polymerase chain reaction (PCR), according to previously described methods.[9,11]

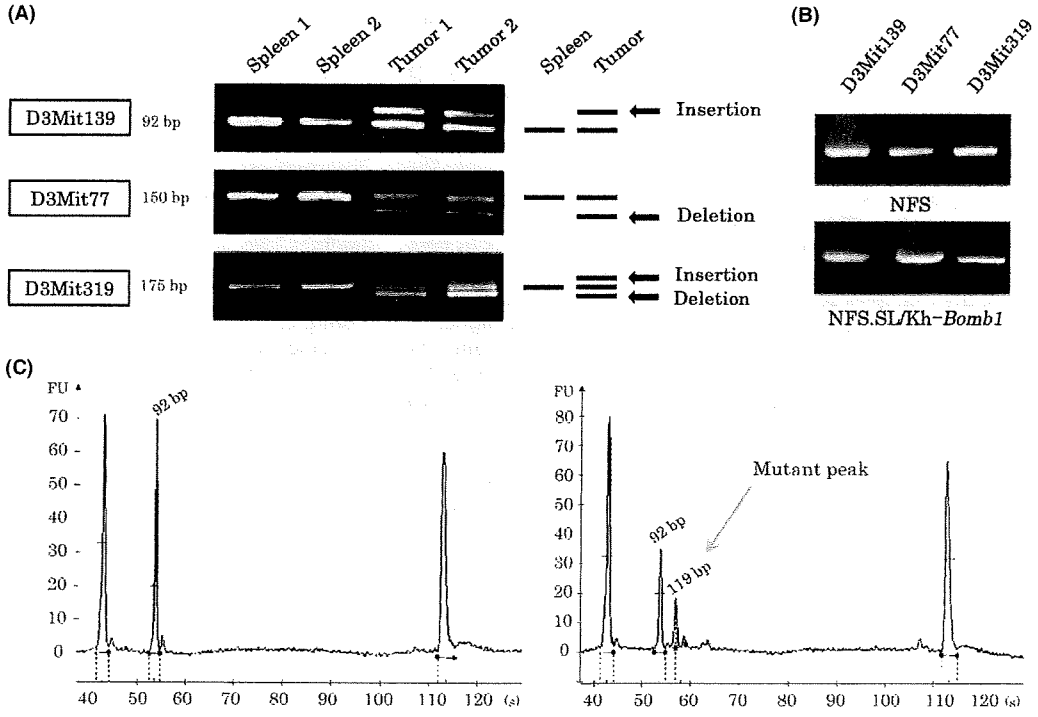

Fig. 1. Microsatellite instability (MSI) screening in SL/Kh B-cell lymphoblastic lymphomas. (A) MSI screening via 3% agarose gel electrophoresis. Agarose gel results obtained at three microsatellite markers showing three variant representations of MSI: insertion mutations resulting from the gain of simple repetitive sequences obtained at marker D3Mit139 (top), deletion mutations (the loss of simple repetitive sequences) observed at marker D3Mit77 (middle), and insertion/deletion mutations (the simultaneous presentation of both insertion and deletion mutations) observed at marker D3Mit319 (bottom). Lanes 1 and 2, SL/Kh spleen-derived polymerase chain reaction (PCR) amplicons from two separate mice (mouse no. 202 and 211).Approximate band sizes are given for healthy control amplicons. Lanes 3 and 4, SL/Kh tumor-derived PCR amplicons demonstrating partial band shifting (mouse no. 202 and 211). (B) Examples of microsatellite stability represented by the external control strains: NFS/N (top) and NFS.SL/Kh-Bomb1 (bottom). Both strains failed to exhibit MSI at any of the examined loci, despite the fact that the introgressed SL/Kh *Bomb1* segment in the NFS.SL/Kh–*Bomb1* strain results in an aberrant polyclonal pro-B cell expansion in bone marrow, mirroring the precursor lesion to lymphomagenesis in SL/Kh mice. Results are shown for markers D3Mit139, D3Mit77, and D3Mit319. (C) Representative allelic profile of SL/Kh spleen and tumor specimens at marker D3Mit139, as analyzed via capillary electrophoresis. Vertical and horizontal scales represent peak fluorescence intensity in relative fluorescence units (FU) and an estimate of PCR product size in base pairs (bp), respectively. The two flanking peaks in each electropherogram are size markers placed at 15 and 1500 bp. Amplicons obtained using normal (splenic) SL/Kh DNA as the template (left). PCR product obtained from tumor DNA showing mutant peak (right; arrow). In normal DNA, a single, dual-intensity homozygous peak is observed, while in tumor amplicons, partial peak shifting is observed and FU is reduced to approximately half the intensity seen in normal tissue.

MSI screening and confirmation. PCR amplicons were subjected to two modes of confirmation for MSI: standard electrophoresis using 3% agarose gel and PCR capillary electrophoresis (Agilent 2100 Bioanalyzer, Palo Alto, CA, USA). The MSI status was established by the presence or absence of aberrant products manifesting in the form of extra bands or peaks, and individually confirmed by two examiners. PCR products with established MSI statuses were further examined under bidirectional sequencing using an ABI3100 automated sequencer and BigDye v3.1 terminators (Applied Biosystems, Foster City, CA, USA) (data not shown).

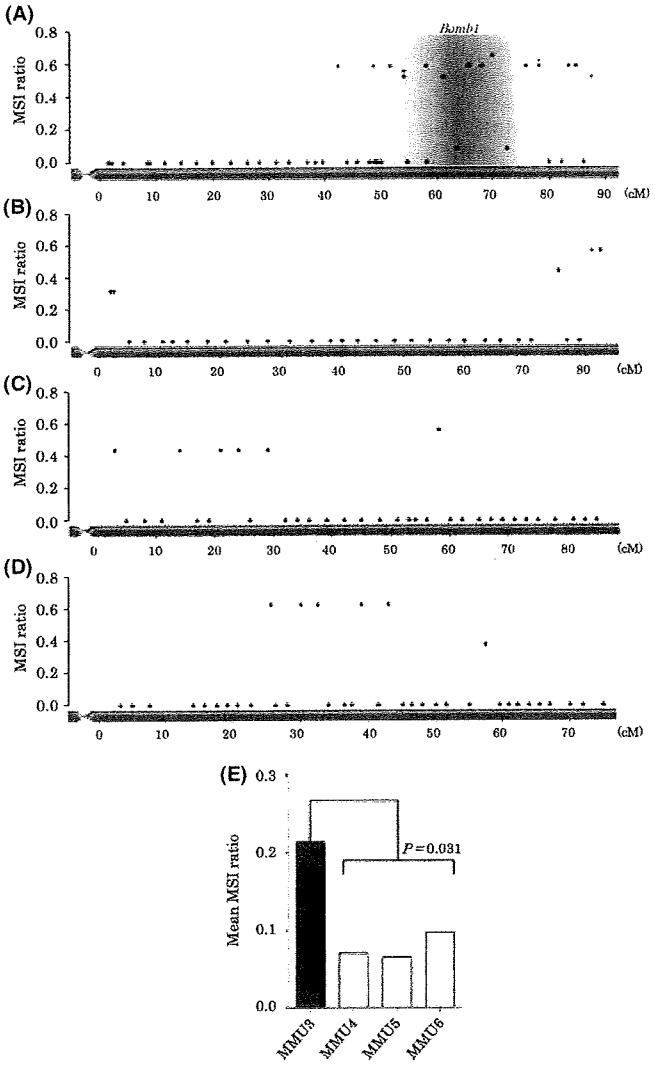

Fig. 2. Transchromosomal comparison of microsatellite instability (MSI) incidence. MSI incidence for each microsatellite marker examined is obtained by dividing the number of MSI-positive samples by the total number of typed lymphoma samples (n = 16). Plots are designed to reflect approximate chromosomal position of each individual microsatellite marker investigated in this study. MSI distribution is shown for the four mouse chromosomes investigated: (A) mus musculus chromosome (MMU)3, (B) MMU4, (C) MMU5, (D) MMU6. *Bomb1* is shaded in gray. Data plots for markers D3Mit300 (55 cM) and D3Mit45 (78.5 cM) representing the boundaries for the *Bomb1* locus are identified on MMU3 with symbols + and *, respectively. Overall MSI incidence was determined for each chromosome by calculating the combined average incidence of MSI per marker on each chromosome (E). cM, centimorgans.

Statistical analysis. To investigate the associations between MSI clustering and the QTL, we applied standard descriptive statistics to characterize data sets. For the comparison of sample groups, a two-tailed Mann–Whitney U-test was used to evaluate statistical significance. A P-value <0.05 was considered to be statistically significant.

***K*-function analysis.** To analyze the distribution patterns of MSI-susceptible loci, we applied a 1-D version of Ripley's K-function.[30] The K-function describes the extent to which there is spatial dependence in the arrangement of events.[31] It is highly useful in identifying the scales at which the spatial point pattern is regarded as significantly underdispersed (clustered) or overdispersed (regular). A certain measure of incidence of MSI at a marker corresponds to an 'event' or point in our study. The K-function analysis is based on distances between all pairs of events, and the function for a point process is defined by:

$$K(t) = \lambda^{-1} E[\text{number of further events within distance } t \text{ of an arbitrary event}] \quad (1)$$

where λ is the intensity, or mean number of events per unit area, and $E[x]$ denotes the expectation of a random variable, x.

Accordingly, the test statistic of $K(t)$ for our analysis was calculated as follows:

$$K(t) = \lambda^{-1} n^{-1} \sum_{i=1}^{n} \sum_{\substack{j=1 \\ (j \neq i)}}^{n} It(u_{ij}) = ln^{-2} \sum_{i=1}^{n} \sum_{\substack{j=1 \\ (j \neq i)}}^{n} It(u_{ij}) \quad (2)$$

where n is the total number of markers susceptible to MSI, l is the combined length (cM) of the four examined chromosomes, u_{ij} is the distance (cM) between points i and j, and $I_t(u)$ and the counter function equals 1 if $u \leq t$ and equals 0 if $u > t$, respectively. For this calculation, we considered the markers of which the rate of MSI incidence was >0.3 as genomic points susceptible to MSI. Since chromosomes are spatially separated, the value of u_{ij} was set to infinite where points i and j represent markers on different chromosomes.

The null hypothesis for our analysis is that every microsatellite locus has an equal probability of showing MSI. Monte Carlo simulation was used to evaluate the significance of deviation from the null hypothesis. The null hypothetical point pattern was realized by randomly choosing n markers among the 150 microsatellite markers that we actually examined.[32] Subsequently, the $K(t)$ for the null hypothetical point pattern was calculated. This was done 1000 times to generate the null distribution. The 95% simulation envelope are the 2.5 and 97.5 percentiles in the null distribution of $K(t)$ for each distance, t.

The values of $K(t)$ can be standardized with the simulated null-distribution as follows:

$$K_{st}(t) = \{K(t) - K_m(t)\}/\sigma(t) \quad (3)$$

where $K_m(t)$ and $\sigma(t)$ are the mean and the standard deviation of the null distribution of $K(t)$. The standardized values of the observed $K(t)$ and the 95% simulation envelope were plotted together against the distance, t. Positive values of standardized K-function, $K_{st}(t)$, for a distance indicate clustering (underdispersion) at the scale of the distance, while negative values indicate regularity (overdispersion). Spatial clustering or regularity at the scale of a distance is statistically significant if the value of the observed $K(t)$ for the distance falls outside the 95% simulation envelope in the plot.

doi: 10.1111/j.1349-7006.2009.01437.x

Results

MSI Screening. B-LBL-derived DNA samples (n = 16) were investigated at each of the 150 microsatellite markers positioned to span the entirety of MMU3–6. These chromosomes were selected on the basis of displaying the closest resemblance to MMU3 in terms of total estimated length (maximum variance 10 Mb), as determined via data retrieved from the MGB.[27] Our genome-wide screening using microsatellite markers revealed three variant representations of MSI in lymphoma-derived DNA: insertions, deletions, and insertion/deletions (Fig. 1A). MSI was observed at 2≤ microsatellite loci in lymphoma-derived DNA obtained from 15 (93.7%) SL/Kh mice; however, no MSI was observed in healthy splenic DNA derived from SL/Kh mice. Thus, the identified mutations in SL/Kh lymphoma-derived DNA are considered to be tumor-specific and not random background instability.[33] Additionally, BM-derived DNA obtained from NFS/N and NFS.SL/Kh–*Bomb1* mice screened in parallel with SL/Kh specimens were consistently negative for MSI at all examined loci (Fig. 1B). In total, 34 (22.6%) of the investigated markers demonstrated discernible MSI in SL/Kh lymphoma-derived DNA, while all others (77.3%) were negative for gross genomic instability. To ascertain the results obtained from our preliminary MSI screening using 3% agarose gel electrophoresis, we retested the samples originally screened as MSI positive via capillary electrophoresis (Fig. 1C).

Table 1. MSI-positive markers

Marker†	MMU‡	Marker position (cM§)	Repeat unit	Mutation phenotype¶	No. MSI-positive samples (%)
D3Mit139	3	43.6	GT	Insertion	9 (56.2)
D3Mit77	3	49.7	GT	Deletion	9 (56.2)
D3Mit343	3	52.5	CA	Insertion	9 (56.2)
D3Mit300	3	55.0	GT	Insertion	8 (50.0)
D3Mit80	3	58.8	CA	Deletion	9 (56.2)
D3Mit319	3	61.8	CA	Insertion/ Deletion	8 (50.0)
D3Mit290	3	64.1	CA	Insertion	1 (7.6)
D3Mit256	3	66.2	GT	Deletion	9 (56.2)
D3Mit291	3	66.2	GT	Deletion	9 (56.2)
D3Mit351	3	68.5	CA	Deletion	9 (56.2)
D3Mit258	3	70.3	CA	Insertion	10 (62.5)
D3Mit113	3	72.0	GT	Insertion	1 (7.6)
D3Mit321	3	76.2	CA	Insertion	9 (56.2)
D3Mit45	3	78.5	GT	Deletion	9 (56.2)
D3Mit352	3	83.5	CA	Deletion	9 (56.2)
D3Mit129	3	84.9	CA	Insertion	9 (56.2)
D3Mit163	3	87.6	GT	Deletion	8 (50.0)
D4Mit64	4	1.9	GT	Insertion	5 (31.2)
D4Mit317	4	2.5	CAAA	Deletion	5 (31.2)
D4Mit233	4	75.5	GT	Insertion	7 (43.7)
D4Mit180	4	81.0	CA	Insertion	9 (56.2)
D4Mit254	4	82.5	GT	Deletion	9 (56.2)
D5Mit331	5	3.0	CA	Deletion	7 (43.7)
D5Mit386	5	14.0	CA	Deletion	7 (43.7)
D5Mit421	5	21.0	CA	Insertion	7 (43.7)
D5Mit77	5	24.0	CA	Deletion	7 (43.7)
D5Mit132	5	29.0	GT	Insertion	7 (43.7)
D3Mit239	5	58.0	GT	Insertion	9 (56.2)
D6Mit275	6	25.5	GT	Insertion	10 (62.5)
D6Mit95	6	30.0	CA	Insertion	10 (62.5)
D6Mit208	6	32.5	GT	Insertion	10 (62.5)
D6Mit249	6	39.0	GT	Insertion	10 (62.5)
D6Mit230	6	43.0	GT	Deletion	10 (62.5)
D6Mit134	6	57.5	GT	Insertion	6 (37.5)

†DNA segment, chromosome no., name of laboratory that discovered the segment (Massachusetts Institute of Technology; MIT), and serial number assigned by order of discovery on each chromosome by the discovering laboratory; ‡mouse chromosome number where marker is located; §marker position on chromosome designated in cM, centimorgans (cM); ¶type of mutation identified at marker: insertion, deletion, or insertion/deletion. MMU, mus musculus chromosome; MSI, microsatellite instability.

Chromosomal MSI distribution and incidence. Our preliminary results showed that MMU3 seemingly harbors a higher overall incidence of MSI, thus we investigated whether the *Bomb1* region is intrinsically more unstable than other autosomal regions of the lymphoma genome. To this end, a framework map was constructed for each of the mouse chromosomes examined, illustrating the approximate chromosomal positions and incidence of MSI-positive samples per marker. The patterns of MSI distribution within the B-LBL genome are given for MMU3-6 in Figure 2(A–D).

MSI incidence per marker was obtained by dividing the number of MSI-positive samples by the total number of B-LBL samples tested (n = 16). Similarly, mean MSI ratios were determined for each chromosome by calculating the combined average incidence of MSI for each marker tested. The overall MSI ratios for MMU3–6 were 0.213 (mean), 0.07, 0.066, and 0.097, respectively. While relatively comparable results were obtained for MMU4, MMU5, and MMU6, significantly higher incidences of MSI ($P = 0.031$) were confirmed on MMU3, which harbors the *Bomb1* locus (Fig. 2E). When the same calculations were performed neglecting the data obtained from the *Bomb1* markers, the overall incidence of MSI on MMU3 (0.116) resembled that of the remaining chromosomes tested ($P = 0.754$). Percentages of MSI-positive B-LBL samples per unstable marker, along with marker position and repeat units, are provided in Table 1. Notably, each of the markers presenting with gross instability displayed total consistency with regard to the type of MSI (insertion, deletion, or insertion/deletion) observed among samples.

Point pattern of MSI-susceptible loci along the chromosomes. The K-function analysis was performed collectively for the four chromosomes examined. The observed point pattern is comprised of 32 microsatellite loci with high MSI incidence (more than 0.3) distributed over the four chromosomes. The standardized version of the observed K-function and the corresponding 95% simulation envelope are shown in Figure 3(A). The observed K-function lies above the 95% simulation envelope at distances from 4 to 50 cM, indicating significant clustering of the MSI-susceptible loci over the range of scales. Spatial clustering is most marked at the scale of 18–20 cM (Fig. 3A), where the extent of deviation from the null distribution is most prominent ($P < 0.002$).

To identify the chromosomal locations of the clustering of MSI-susceptible loci, we calculated local frequencies of loci relative to that of the microsatellite markers for each segment of the scale at which clustering was most marked (=19 cM) and mapped them over the chromosomes. In Figure 3(B), for each genomic position, a value is plotted that indicates the observed count of MSI-susceptible loci within 19 cM of the position divided by the count of the actually examined microsatellite markers within the same segment. To correct the edge effect, for the region beyond the terminus of a chromosome, the ratio of frequency of MSI-susceptible loci to microsatellite markers was assumed to be constantly equal to the expected ratio (=32/150). The shaded areas cover the genomic positions that display a ratio of frequencies above the expected ratio, which denotes clustering of MSI-susceptible loci. A region demonstrating the most extensive clustering is clearly recognized toward the telomere of MMU3.

Discussion

The results obtained from our genome-wide screening and spatial point pattern analysis clearly indicate the presence of MSI-susceptible loci forming clusters across the lymphoma genome. While the *Bomb1* locus is the most outstanding example of the clustering of MSI-susceptible loci, similar patterns of cluster distribution, albeit on a smaller scale, were duly noted on the other chromosomes we investigated as well.

The preliminary results we obtained advocate the theory that the *Bomb1* locus harbors a greater number of MSI-susceptible loci over other autosomal regions of the genome; however, the full range of instability in the B-LBL genome will not be apparent until more samples are dissected at the fine-scale level. Similarly, while the strength of this study lies in the large number of markers tested and meticulous screening methods, it is conceivable that we might have improved our chances of detecting MSI in the *Bomb1* locus in greater quantities owing to the greater number of markers being tested on MMU3. This was due to the increased availability of markers on MMU3 from the original QTL analyses performed on *Bomb1*.

One of the striking features associated with this study was the uniformity of MSI manifestation obtained at each of the MSI presenting markers. Numerous studies have shown that the healthy genome of inbred strains display apparent polymorphisms in genomic copy number[34–36] and other genetic differences;[37] however, to our knowledge, this is the first study to extensively document the uniformity of post-tumorigenic mutations in the cancer genome of a well-maintained inbred strain of mice.

The rapidly expanding repertoire of MSI-associated malignancies warrants further investigation into the individual characteristics of MSI distribution in diverse cancer genomes. This bears significant value to researchers and clinicians alike, for the presence or absence of the MSI phenotype in a defined subset of cancers has monumental impact on the clinical prognosis and treatment of patients.[38–40] Additionally, because MSI investigations on humans have been incremental rather than groundbreaking, similar studies encompassing a variety of laboratory animals and strains could aide in deciphering the code for the biological mechanism governing MSI manifestation in mammalian malignant neoplasms. The results of this and similar studies characterizing MSI in a broad spectrum of cancers could lead to the advent of disease-specific MSI panels, and further holds the possibility of uncovering the existence of heritable patterns of post-tumorigenic genomic instability in mammals.

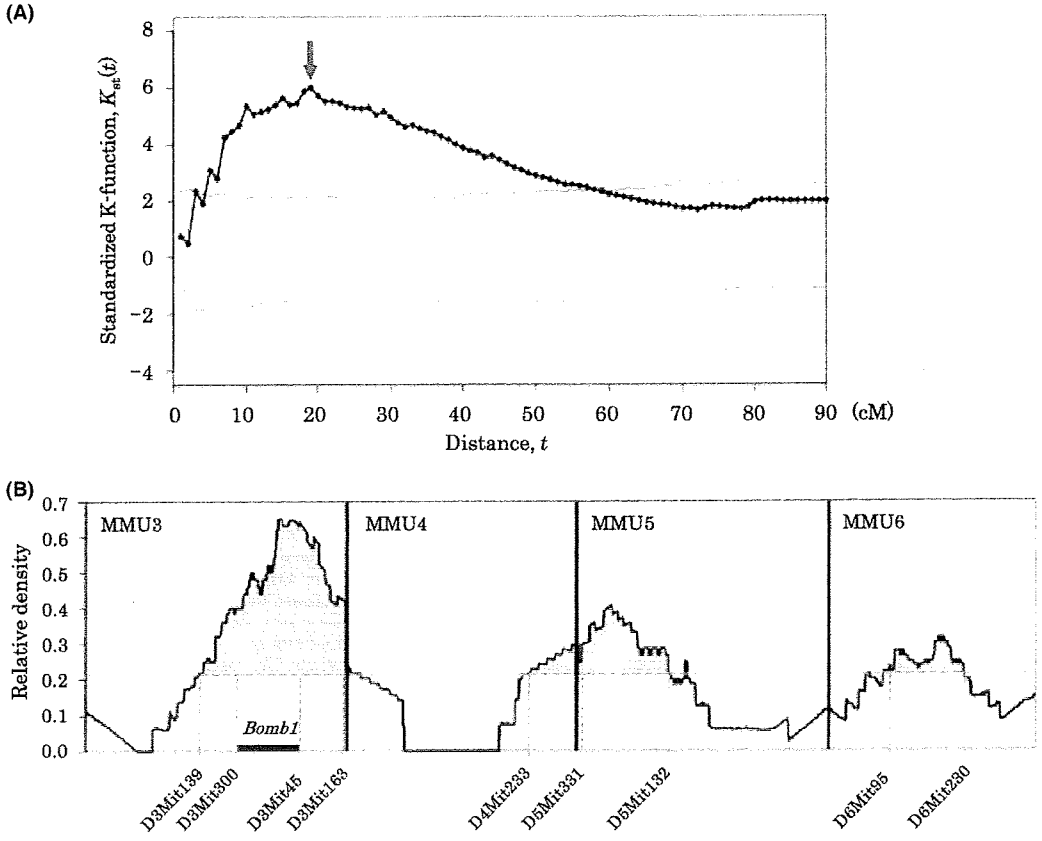

Fig. 3. Spatial point pattern analysis. Point pattern analysis for the distribution of microsatellite instability (MSI)-susceptible loci along the chromosomes. (A) Plot of standardized *K*-function for observed data (dark line) and 95% simulation envelope (gray lines). Statistical significance of the clustering of MSI-susceptible loci is shown at the 0.05 level for distance, *t* (cM), where portions of the dark line stray above the upper gray line. Arrow indicates the point at which the observed *K*-function deviates maximally from the null distribution for equal probabilities. (B) Chromosomal map of local density of MSI-susceptible loci in the scale showing most significant clustering (=19 cM). *Y*-axis indicates the observed count of MSI-susceptible loci within 19 cM of each chromosomal position divided by the count of the actually examined microsatellite markers within the same segment. Dashed line denotes overall density (=32/150). Shaded areas represent genomic positions displaying a ratio of frequencies above the expected ratio (clustering). A region demonstrating the most extensive clustering is clearly recognized in the vicinity of the *Bomb1* locus on mus musculus chromosome (MMU)3. cM, centimorgans.

doi: 10.1111/j.1349-7006.2009.01437.x

Acknowledgments

This work was supported by a Grant-in-Aid for Cancer Research from the Ministry of Education, Culture, Sports, Science, and Technology, Japan, and a Grant for Strategic Research on Cancer from the Ministry of Health, Labor, and Welfare, Japan. Additionally, we are grateful for the generous financial support provided by the Kyoto Shimizu Immunology Foundation. Lastly, we wish to thank Mr. Chihiro Kawai, Ms. Yukiko Imai, Mr. Haruya Takeuchi and Ms Hiroko Saito at the Department of Forensic Medicine and Molecular Pathology, Kyoto University Graduate School of Medicine for their technical assistance.

References

1 Soslow RA, Baergen RN, Warnke RA. B-Lineage lymphoblastic lymphoma is a clinicopathologic entity distinct from other histologically similar aggressive lymphomas with blastic morphology. *Cancer* 1999; **85**: 2648–54.
2 Cheng A-L, Su I-J, Tien H-F, Wang C-C, Chen Y-C, Wang C-H. Characteristic clinicopathologic features of adult B-cell lymphoblastic lymphoma with special emphasis on differential diagnosis with an atypical form probably of blastic lymphocytic lymphoma of intermediate differentiation origin. *Cancer* 1994; **73**: 706–10.
3 Sander CA, Jaffe ES, Gebhardt FC, Yano T, Medeiros LJ. Mediastinal lymphoblastic lymphoma with an immature B-cell immunophenotype. *Am J Surg Pathol* 1992; **16**: 300–5.
4 Link MP, Roper M, Dorfman RF, Crist WM, Cooper MD, Levy R. Cutaneous lymphoblastic lymphoma with pre-B markers. *Blood* 1983; **61**: 838–41.
5 Pattengale PK, Frith CH. Immunomorphologic classification of spontaneous lymphoid cell neoplasms occurring in female BALB/c mice. *J Natl Cancer Inst* 1983; **70**: 169–79.
6 Hiai H, Kaneshima H, Nakamura H, Oguro BY, Moriwaki K, Nishizuka Y. Unusually early and high rate of spontaneous occurrence of nonthymic leukemias in SL/Kh mice, a subline of SL strain. *Jpn J Cancer Res* 1982; **73**: 603–13.
7 Hiai H, Tsuruyama T, Yamada Y. Pre-B lymphomas in SL/Kh mice: a multifactorial disease model. *Cancer Sci* 2003; **94**: 847–50.
8 Shimada MO, Yamada Y, Nakakuki Y *et al.* SL/Kh strain mice: a novel animal model of pre-B lymphomas. *Leuk Res* 1993; **17**: 573–8.
9 Okamoto K, Yamada Y, Shimada MO, Nakakuki Y, Nomura H, Hiai H. Abnormal bone marrow B-cell differentiation in pre-B lymphoma prone SL/Kh mice. *Cancer Res* 1994; **54**: 399–402.
10 Lu LM, Shimada M, Higashi S, Zeng ZZ, Hiai H. Bone marrow pre-B-1 (*Bomb1*): a quantitative trait locus inducing bone marrow pre-B 1 cell expansion in lymphoma-prone SL/Kh mice. *Cancer Res* 1999; **59**: 2593–5.
11 Hiratsuka T, Tsuruyama T, Kaszynski R *et al.* Bone marrow pre-B expansion by SL/Kh-Bomb1 locus: not sufficient for lymphomagenesis. *Leuk Res* 2008; **32**: 309–14.
12 Aaltonen LA, Peltomaki P, Leach FS *et al.* Clues to the pathogenesis of familial colorectal cancer. *Science* 1993; **260**: 812–6.
13 Thibodeau SN, Bren G, Schaid D. Microsatellite instability in cancer of the proximal colon. *Science* 1993; **260**: 816–9.
14 Eshleman JR, Markowitz SD. Mismatch repair defects in human carcinogenesis. *Hum Mol Genet* 1996; **5**: 1489–94.
15 Ionov Y, Peinado MA, Malkhosyan S, Shibata D, Perucho M. Ubiquitous somatic mutations in simple repeated sequences reveal a new mechanism for colonic carcinogenesis. *Nature* 1993; **363**: 558–61.
16 Moslein G, Tester DJ, Lindor NM *et al.* Microsatellite instability and mutation analysis of hMSH2 and hMLH1 in patients with sporadic, familial and hereditary colorectal cancer. *Human Mol Genet* 1996; **5**: 1245–52.
17 Burks RT, Kessis TD, Cho KR, Hedrick L. Microsatellite instability in endometrial carcinoma. *Oncogene* 1994; **9**: 1163–6.
18 Mironov NM, Aguelon MA-M, Potapova GI *et al.* Alteration of (CA)n DNA repeats and tumor suppressor genes in human gastric cancer. *Cancer Res* 1994; **54**: 41–4.
19 Shridhar V, Siegfried J, Hunt J, Alonso M, Smith DI. Genetic instability of microsatellite sequences in many non-small cell lung carcinomas. *Cancer Res* 1994; **54**: 2084–7.
20 Uchida T, Wada C, Wang C, Egawa S, Ohtani H, Koshiba K. Genomic instability of microsatellite repeats and mutations of H-, K-, and N-ras and p53 genes in renal cell carcinoma. *Cancer Res* 1994; **54**: 3682–5.
21 Yee JC, Roodi N, Verrier C, Parl FF. Microsatellite instability and loss of heterozygosity in breast cancer. *Cancer Res* 1994; **54**: 1641–4.
22 Niv E, Bomstein Y, Bernheim J, Lishner M. Microsatellite instability in gastric MALT lymphoma. *Mod Pathol* 2004; **17**: 1407–13.
23 Han HJ, Yanagisawa A, Kato Y, Park JG, Nakamura Y. Genetic instability in pancreatic cancer and poorly differentiated type of gastric cancer. *Cancer Res* 1993; **53**: 5087–9.
24 Gonzalez-Zulueta M, Ruppert JM, Tokino K *et al.* Microsatellite instability in bladder cancer. *Cancer Res* 1993; **53**: 5620–3.
25 Gurin CC, Federici MG, Kang L, Boyd J. Causes and consequences of microsatellite instability in endometrial carcinoma. *Cancer Res* 1999; **59**: 462–6.
26 Hanford MG, Rushton BC, Gowen LC, Farber RA. Microsatellite mutation rates in cancer cell lines deficient or proficient in mismatch repair. *Oncogene* 1998; **16**: 2389–93.
27 Bult CJ, Eppig JT, Kadin JA *et al.* The Mouse Genome Database (MGD): mouse biology and model systems. *Nucleic Acids Res* 2008; **36**: D724–8. [Cited 1 Nov 2008.] Available from URL: http://www.informatics.jax.org/mgihome/other/mouse_facts1.shtml
28 Chattopadhyay SK, Lowy DR, Teich NM, Levine AS, Rowe WP. Evidence that the AKR murine leukemia virus genome is complete in DNA of the high-virus AKR mouse and incomplete in the DNA of the "virus-negative" NIH mouse. *Proc Natl Acad Sci USA* 1974; **71**: 167–71.
29 Fredrickson TN, Morse HC III, Rowe WP. Spontaneous tumors of NFS mice congenic for ecotropic murine leukemia virus induction loci. *J Natl Cancer Inst* 1984; **73**: 521–4.
30 Kraft CE, Warren DR. Development of spatial pattern in large woody debris and debris dams in streams. *Geomorphology* 2003; **51**: 127–39.
31 Ripley BD. The second-order analysis of stationary point processes. *J Appl Probab* 1976; **13**: 255–66.
32 Ersbøll AK, Ersbøll BK. Simulation of the K-function in the analysis of spatial clustering for non-randomly distributed locations – exemplified by bovine virus diarrhoea virus (BVDV) infection in Denmark. *Prev Vet Med* 2009; **91**: 64–71.
33 Weber JL, Wong C. Mutation of human short tandem repeats. *Hum Mol Genet* 1993; **2**: 1123–8.
34 Watkins-Chow DE, Pavan WJ. Genomic copy number and expression variation within the C57BL/6J inbred mouse strain. *Genome Res* 2008; **18**: 60–6.
35 Li J, Jiang T, Mao J-H *et al.* Genomic segmental polymorphisms in inbred mouse strains. *Nat Genet* 2004; **36**: 952–4.
36 Snijders AM, Nowak NJ, Huey B *et al.* Mapping segmental and sequence variations among laboratory mice using BAC array CGH. *Genome Res* 2005; **15**: 302–11.
37 Specht CG, Schoepfer R. Deletion of the alpha-synuclein locus in a subpopulation of C57BL/6J inbred mice. *BMC Neurosci* 2001; **2**: 11.
38 Sankila R, Aaltonen LA, Jarvinen HJ, Mecklin JP. Better survival rates in patients with MLH1-associated hereditary colorectal cancer. *Gastroenterology* 1996; **110**: 682–7.
39 Kohonen-Corish MR, Daniel JJ, Chan C *et al.* Low microsatellite instability is associated with poor prognosis in stage C colon cancer. *J Clin Oncol* 2005; **23**: 2318–24.
40 Wright CM, Dent OF, Newland RC *et al.* Low level microsatellite instability may be associated with reduced cancer specific survival in sporadic stage C colorectal carcinoma. *Gut* 2005; **54**: 103–8.

Supporting Information

Additional Supporting Information may be found in the online version of this article:

Data S1. Markers examined in this study are as follows (values in parentheses denote chromosomal position in cM).

Please note: Wiley-Blackwell are not responsible for the content or functionality of any supporting materials supplied by the authors. Any queries (other than missing material) should be directed to the corresponding author for the article.

Epub ahead of print April 1, 2010 - doi:10.1189/jlb.1109748

JLB

Article

Dual retrovirus integration tagging: identification of new signaling molecules *Fiz1* and *Hipk2* that are involved in the IL-7 signaling pathway in B lymphoblastic lymphomas

Tatsuaki Tsuruyama,[*,1] Yukiko Imai,*[*] Haruya Takeuchi,*[*] Takuya Hiratsuka,*[†] Yasuhiro Maruyama,*[‡] Kazuya Kanaya,*[‡] Richard Kaszynski,*[*] Guang Jin,*[§] Tomoko Okuno,*[*] Munetaka Ozeki,*[*] Takuro Nakamura,*[§] Tetsuya Takakuwa,*[‡] Toshiaki Manabe,*[†] Keiji Tamaki,*[*] and Hiroshi Hiai*[‖]

*Department of Forensic Medicine and Molecular Pathology and †Department of Diagnostic Pathology, and ‡Department of Human Health Science, Graduate School of Medicine, Kyoto University, Kyoto, Japan; §Laboratory of Carcinogenesis, Cancer Institute, Tokyo, Japan; and ‖Shiga Medical Center Research Institute, Shiga, Japan

RECEIVED NOVEMBER 9, 2009; REVISED FEBRUARY 11, 2010; ACCEPTED MARCH 5, 2010. DOI: 10.1189/jlb.1109748

ABSTRACT

IL-7R, FLT3, and CD43 are surface antigens expressed during the transition from pro-B to pre-B cells in BM. To understand interactions between their signaling pathways, we analyzed spontaneous mouse B-LBLs with dual MLV integration into *Stat5a* and *Fiz1* or *Stat5a* and *Hipk2*. MLV integration resulted in up-regulation of these genes in lymphoma cells compared with normal pro-B cells from the BM. In lymphomas with both integrations into *Stat5a* and *Fiz1*, increases in phosphorylated STAT5A and expression of c-Myc, a target gene of STAT5A, were observed following stimulation of the FLT3. Clones with the dual integrations grew faster in IL-7 and FLT3L-supplemented medium than clones with *Stat5a* integration alone. On the other hand, in lymphomas with integrations into *Stat5a* and *Hipk2*, increases in phosphorylated STAT5A and expression of c-Myc were observed following cross-linking of CD43. In conclusion, FLT3 and CD43 signaling pathways involve STAT5A via *Fiz1* and *Hipk2* in B-LBLs. Identification of the dual MLV integration sites in B-LBLs, therefore, will provide an excellent tool for identification of the signaling pathways in B-LBLs. *J. Leukoc. Biol.* 88: 000–000; 2010.

Introduction

Retroviral insertional mutagenesis in several inbred strains of mice induces a high incidence of myeloid leukemia and B and T cell lymphomas, as well as other types of tumors [1]. The retroviral integration sites in these tumors thus provide powerful tools for the identification of novel oncogenes and tumor-related genes [2]. The inbred strain of mice SL/Kh develops lymphoma spontaneously as a result of genetically acquired MLV integration [3, 4]. More than 90% of these mice develop $B220^+$ $BP\text{-}1^+$ $CD43^+$ $CD24^+$ $sIgM^-$ B-LBLs spontaneously by 6 months of age [5]. As development of spontaneous B-LBLs is rare in most other mice, the SL/Kh strain is an important model for studying the pathogenesis of B-LBLs. By analyzing (SL/Kh×NFS/N) × NFS/N F2, we have mapped a highly significant quantitative trait locus, named Bomb1, on the distal segment of mouse chromosome 3, which is responsible for pre-B expansion [6]. NFS/N is an inbred mouse strain without an endogenous, ecotropic MLV genome and with low spontaneous lymphoma incidence [7]. We generated a congenic strain, NFS/N.SL/Kh-Bomb1 mice, in which the Bomb1 locus is replaced by the identical locus in the SL/Kh mice genome. We observed that the congenic mice showed pre-B cell expansion after 4 months of the birth and demonstrated that the Bomb1 locus is crucial for the pre-B expansion [8]. Such spontaneous lymphoma strains have been used as a tool to search for novel oncogenes by identification of common integration sites of MLV [1, 2]. Reintegration of endogenous MLV genomes into the cancer-related genes *Stat5a* [9] and *c-myc* [10] induced these lymphomas. In this study, we show that these mice are also a useful model for investigation of oncogene pathway interactions by analysis of lymphomas with dually integrated, clonal MLVs. Wu et al. [11] reported that MLV integration favors transcriptionally active genes. Therefore, when lymphoma cells have more than one clonally integrated MLV ge-

Abbreviations: B-LBL=B-lymphoblastic lymphoma, BM=bone marrow, Bomb1=bone marrow pre-B-1, D_H-J_H=Ig heavy chain diversity-joining, *Emv11*-endogenous ecotropic MuLV11, *Fiz1*= fms-like tyrosine kinase 3-interacting zinc finger protein 1, FLT3L=fms-like tyrosine kinase 3 ligand, *Hipk2*=CD43-interacting homeodomain-interacting protein kinase 2, *IgH*=Ig heavy chain, *IgL*=Ig light chain, ITD=internal tandem duplication, MLV=murine leukemia retrovirus, sIgM=surface IgM

1. Correspondence: Department of Forensic Medicine and Molecular Pathology, Graduate School of Medicine, Yoshida-konoe-cho, Sakyo-ku, Kyoto 606-8501, Japan. E-mail: tsuruyam@kuhp.kyoto-u.ac.jp

nome, the host genes are likely to be commonly active, and their interaction can be observed in the host cells. We reported previously that one of the common integration sites of MLV in SL/Kh B-LBLs is *Stat5a*, whose constitutive activation is responsible for pre-B cell lymphomagenesis in vivo and in vitro [9]. Activated STAT5A forms a dimer and influences transcriptional activity of other genes by binding to the γ-activated site element in the promoter of target antiapoptotic genes, such as *c-myc*, *pim-1*, *bcl-xL*, and *cyclin D1* [12–15]. STAT5A is recruited in the IL-7R pathway that operates selectively during the precursor stage of the pro- to pre-B cell transition in BM, as well as in T cells [15, 16].

In the current study, we show two novel types of signaling pathways that were activated by MLV integration. We also identify a novel pathway involved in cellular signaling transmission by analysis of the signaling pathways. We examined the *c-myc* expression via the STAT5A phosphorylation [9]. STAT5 is essential for early B cell development but not for B cell maturation and function [17]. This IL-7R pathway is key in pro-B cell development and is known to regulate IgH recombination and B cell precursor expansion [18, 19]. STAT5 and IL-7 signaling control cell survival and the developmental ordering of Ig gene rearrangements by suppressing premature Igκ recombination in pro-B cells [20]. Thus, the occurrence of B-LBLs in SL/Kh mice caused by *Stat5a* integration is a promising model for investigation of one of the signaling pathways in early B lymphocytes [5]. The development stage of B cells was according to Hardy's standard classification of murine B cell lineage [21]. In the current study, we identified novel integration sites in SL/Kh B-LBLs including *Fiz1* and *Hipk2*. *Fiz1* encodes a novel zinc finger protein with C_2H_2-type zinc fingers that interacts with the receptor tyrosine kinase FLT3 [22], a surface antigen of pro- to pre-B cells. On the other hand, *Hipk2* encodes a member of a novel family of serine/threonine kinases [23] that interacts with the cytoplasmic domain of CD43, which is expressed on most hematopoietic cells, including pro- to pre-B cells. Although the host genes activated by MLV integration were different, the type of lymphoma was consistently B-LBLs. This suggests that cross-talk may be involved in the intracellular pathways activated by the MLV integration. As several clones of cells from SL/Kh B-LBLs had dual *Stat5a* and *Fiz1* or *Stat5a* and *Hipk2* integrations, we studied the cross-talk among signaling molecules in the IL7-R pathway. These data provide novel insights into the pathogenesis of B-LBLs.

MATERIALS AND METHODS

Animals

The origin, endogenous MLVs, and host genetic factors in lymphomagenesis in SL/Kh mice have been reported previously [3–6]. All animal experiments were carried out with approval from the Ethical Committee for Animal Experiments, Kyoto University Graduate School of Medicine (Japan).

Inverse PCR for identification of MLV integration sites

The virus-host junctions of the MLV integration site were amplified with inverse PCR [9]. In brief, genomic DNA (100 ng) from each lymphoma was digested with *Sac*II for 2 h and self-ligated with T4 ligase (Takara Bio, Otsu, Japan) at 14°C overnight. PCR amplification was carried out in three steps in a thermal cycler (Takara Bio) under the following conditions: initial denaturation (1 min at 95°C); then 10 cycles (30 s at 94°C, 40 s at 62°C, and 4 min at 68°C; step 1); then 20 cycles (30 s at 94°C, 40 s at 62°C, and 4 min plus extension of 20 s in one cycle at 68°C; step 2); and finally, elongation (10 min at 72°C). In some cases, nested PCR was added to the above reaction. The primers for inverse PCR were located within the MLV genomes. Their

TABLE 1 *Phenotypic Features of Lymphoma*

			IgH								
ID	Sex	Age	D_HJ_H	V_HD_H	IgL	CD43	IL-7R	CD24	V_{preb}	λ5	Integration site
1	f	6	c	n.d.	g	+	+	+	+	–	*Stat5a*
2	m	7	c	n.d.	g	+	+	+	+	–	*Stat5a*
3	f	4	c	n.d.	g	+	+	+	+	–	*Stat5a*
4	m	6	c	c	g	+	+	+	+	–	*Stat5a*
5	f	7	c	c	g	+	+	+	+	–	*Stat5a*
6	f	6	c	c	g	+	+	+	+	–	*Stat5a*
7	m	7	c	n.d.	g	+	+	+	+	–	*Fiz1* + *Stat5a*
8	f	6	c	n.d.	g	+	+	+	+	–	*Fiz1* + *Stat5a*
9	f	10	c	n.d.	g	+	+	+	+	–	*Fiz1* + *Stat5a*
10	m	5	c	n.d.	g	+	+	+	+	–	*Fiz1* + *Stat5a*
11	m	4	c	c	g	+	+	+	+	–	*Fiz1* + *Stat5a*
12	f	9	c	c	g	+	+	+	+	+	*Fiz1*
13	m	6	c	c	g	+	+	+	+	+	*Fiz1*
14	f	7	c	c	g	+	+	+	+	+	*Fiz1*
15	f	5	c	c	g	+	+	+	+	+	*Hipk2*
16	m	8	c	n.d.	g	+	+	+	+	–	*Hipk2*
17	f	4	c	n.d.	g	+	+	+	+	–	*Hipk2* + *Stat5a*
18	m	5	c	c	g	+	+	+	+	–	*Hipk2* + *Stat5a*
19	f	6	c	c	g	+	+	+	+	–	*Hipk2* + *Stat5a*
20	m	7	c	c	g	+	+	+	+	–	*Hipk2* + *Stat5a*
21	m	3	c	c	g	+	+	+	+	–	*Hipk2* + *Stat5a*

f, Female; m, male; c, completed (D_HJ_H); n.d., not detected (V_HD_H); g, germ line (IgL); V_HD_H, variable of IgH.

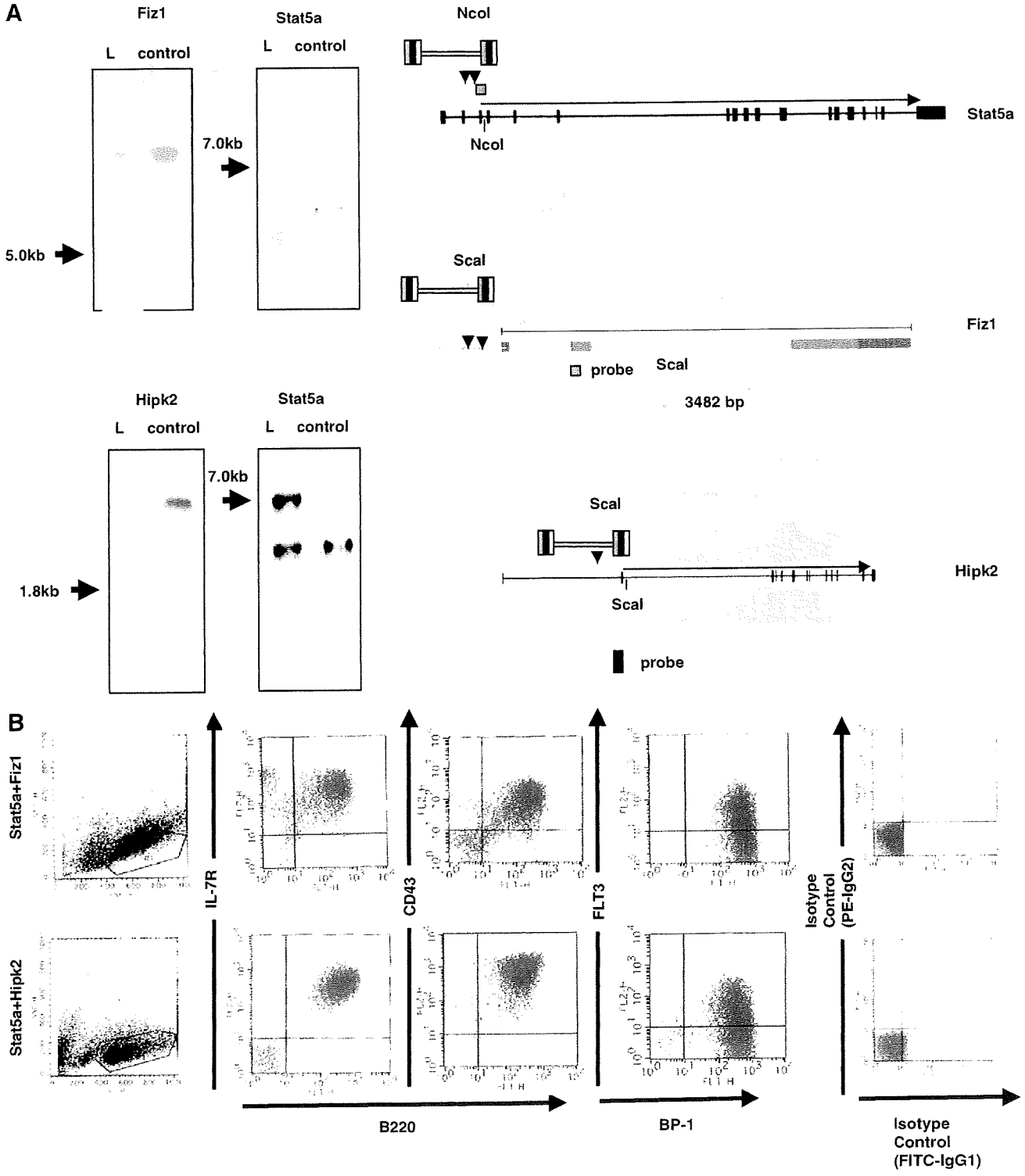

Figure 1. Clonality of B-LBL cells with dual integration. (A) Southern hybridization of LBL cells with *Stat5a* and *Fiz1* or *Stat5a* and *Hipk2* integration. The right scheme shows *Nco*I and *Sca*I sites within the MLV genome and immediately near the third exon of the *Stat5a* gene. The fragments of MLV-mouse genome DNA were visualized on the blot (indicated by arrows), and in these blots, the intensity of the fragments from provirus-integrated *Fiz1* and *Hipk2* was nearly identical to that of fragments from the nonintegrated allele. (B) Flow cytometry analysis of B-LBL cells with dual integration into *Stat5a* and *Fiz1* or *Stat5a* and *Hipk2*. FL2-H, Fluorescence 2-height. *(continued on next page)*